Deep-Sea Research II 65-70 (2012) 126–140

Contents lists available at SciVerse ScienceDirect

Deep-Sea Research II

journal homepage: www.elsevier.com/locate/dsr2

Spatial and seasonal variability of primary production on the Eastern Bering Sea shelf

M.W. Lomas [a,*], S.B. Moran [b], J.R. Casey [a,1], D.W. Bell [a], M. Tiahlo [a,2], J. Whitefield [c], R.P. Kelly [b], J.T. Mathis [c], E.D. Cokelet [d]

[a] Bermuda Institute of Ocean Sciences, 17 Biological Station, St. George's, GE01, Bermuda
[b] Graduate School of Oceanography, University of Rhode Island, Narragansett, RI 02882-1197, USA
[c] School of Fisheries and Ocean Sciences, University of Alaska, Fairbanks, AK 99775-7220, USA
[d] National Oceanic and Atmospheric Administration, Pacific Marine Environmental Lab, Seattle, WA 98115, USA

ARTICLE INFO

Available online 9 February 2012

Keywords:
Bering Sea
Primary production
Seasonal variability
VGPM primary production model

ABSTRACT

Spatial and seasonal variability in net primary production (NPP) is reported for the Eastern Bering Sea shelf in spring and summer 2008 and 2009. Euphotic zone integrated NPP in the spring, estimated from simulated in situ ^{14}C-incubations, varied ~30-fold across the northern and southern regions of the Inner, Middle, and Outer domains of the shelf. During spring, rates were lowest and similar in the North and South region of the Inner domain, while the highest rates were in the Southern region of the Outer domain as a result of extensive ice-edge phytoplankton blooms. Generally, phytoplankton integrated chlorophyll (Chl-a) standing stocks were dominated (>50%) by large (>5 μm) cells. With the exception of the southern Middle domain, integrated rates of NPP were consistently lower in summer than spring, while there was no consistent pattern in changes in integrated Chl-a. Conversely, phytoplankton growth rates (μ) were lower in spring ($0.22 \pm 0.09\ d^{-1}$) than summer ($0.42 \pm 0.17\ d^{-1}$), consistent with a seasonal shift from a biomass-controlled production system to a growth-rate controlled production system. Associated with this shift in control was a decrease in the size distribution of chlorophyll from ~60% of the Chl-a > 5 μm in the spring to ~30% of the Chl-a > 5 μm in the summer. Despite the widespread distribution of stations, these observations highlight the variable nature of NPP in the Bering Sea, which makes the estimation of seasonal or annual rates in any domain or across the entire shelf difficult, if not impossible, on direct observations alone. A vertically generalized productivity model (VGPM) was used to assimilate the more extensive underway dataset from two cruises to improve the spatial distribution of calculated NPP included in the regional estimates of NPP. The VGPM output captured ~83% of the variance in measured ^{14}C production, accurately estimated observed NPP (Model II regression slope ± stdev.; 0.92 ± 0.06), and allowed for a better constrained estimation of shelf-wide productivity due to higher data density in each region/domain. These results, when combined with published data on shelf-wide productivity suggest that the ecosystem response to climate change (whether an increase or decrease in productivity) would have to exceed a factor of two from mean conditions before being detectable from a comparable survey effort.

1. Introduction

Arctic and sub-Arctic seas (e.g., Norwegian/Greenland Seas, Labrador Sea, and Bering Sea) are characterized by high biological productivity and the seasonal presence of sea ice (Hunt and Drinkwater, 2005). In the Eastern Bering Sea shelf ecosystem, the presence or absence of seasonal sea ice is the single most important parameter that determines the physical and biological structure of the water column, not only in the spring, but for the remainder of the growing season (Hunt et al., 2008, 2002; Stabeno et al., 2012-a, 2010). The Bering Sea and other sub-Arctic and Arctic waters are predicted to be among those most severely affected by global warming as relatively small changes in the heat

* Corresponding author. Tel.: +1 441 297 1880; fax +1 441 297 8143.
E-mail addresses: Michael.Lomas@bios.edu (M.W. Lomas), moran@gso.uri.edu (S.B. Moran), jrcasey@hawaii.edu (J.R. Casey), Doug.Bell@bios.edu (D.W. Bell), tiahlo@college.usc.edu (M. Tiahlo), jonathan.whitefield@gmail.com (J. Whitefield), rokelly@gso.uri.edu (R.P. Kelly), jmathis@sfos.uaf.edu (J.T. Mathis), Edward.D.Cokelet@noaa.gov (E.D. Cokelet).
[1] Current address: Department of Oceanography, University of Hawaii—Manoa, Honolulu, HI 96822, USA.
[2] Current address: Department of Biological Sciences, University of Southern California, Los Angeles, CA 90089-0371, USA.

0967-0645/$ - see front matter © 2012 Elsevier Ltd. All rights reserved.
doi:10.1016/j.dsr2.2012.02.010

content of the water column can have a disproportionately large effect on the spatial distribution and dynamics of sea ice (e.g., Meier et al., 2005; Overpeck et al., 2005; Sarmiento et al., 2004). Indeed, increases in regional temperatures have begun to affect the areal extent, concentration, and thickness of ice in both the polar regions and sub-Arctic seas (IPCC, 2007), and further changes in sea-ice extent due to either climate oscillations or global warming will likely have significant impacts on these economically important ecosystems (e.g., Hunt et al., 2010, 2011; Napp and Hunt, 2001; Schumacher et al., 2003).

The Eastern Bering Sea shelf is a physically dynamic environment. During winter, the entire shelf is well mixed to depths of ~100 m. In the summer, fronts divide the Bering Sea shelf into three distinct hydrographic regions: the Inner, Middle and Outer domains (e.g., Coachman, 1986; Coachman and Charnell, 1979; Kachel et al., 2002; Kinder and Coachman, 1978). The Inner Front, roughly overlying the 50 m isobath (Kachel et al., 2002), divides the Inner domain from the Middle domain (Fig. 1). The shallow Inner domain is unstratified even in summer due to mixing of the upper and lower portions of the water column by wind and tides, respectively. The middle front is a broad transitional zone between the 80 m and 100 m isobaths (Coachman, 1986) that separates the Middle and Outer domains. In summer the Middle domain is a two-layered system with an upper wind mixed layer separated from the deeper tidally-mixed layer by a seasonal pycnocline at 15–35 m depth. In the southern portion of the Middle Domain, the pycnocline gradient is sufficiently sharp that sub-surface Chl-a maxima rarely form, whereas in the northern portion, mixing is not as intense and the pycnocline gradient less sharp allowing for formation of sub-surface Chl-a maxima in summer (Stabeno et al., 2012-a). The Outer domain, from 100 m to ~200 m depth, consists of a wind mixed surface layer and a tidally-mixed bottom layer, separated by a transition zone. In addition to the across shelf gradient these domains can be further divided into Northern and Southern regions with a demarcation at ~60°N (Stabeno et al., 2012-a, 2010). The geographical domain notation described here is consistent with other recent studies of the carbon cycle and biological production in this region (e.g., Mathis et al., 2010).

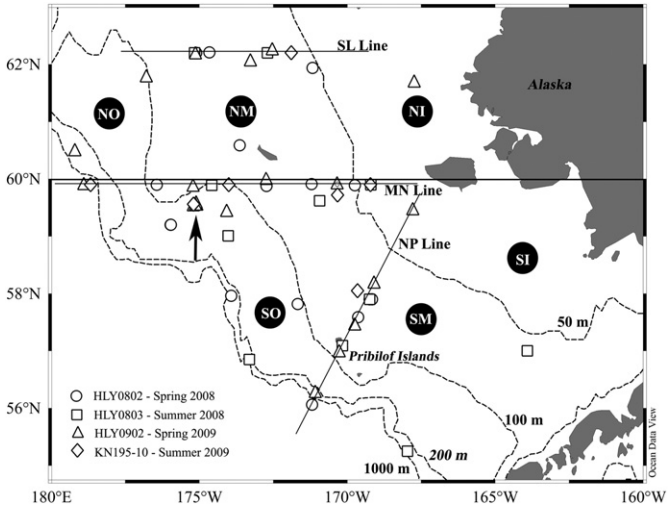

Fig. 1. Study region with process stations identified by the symbols given in the legend. The 50 m, 100 m, and 200 m isobaths are labeled and shown as dashed lines to denote the demarcation between the Inner and Middle domains, the Middle and Outer domains, and the Outer domain and shelf break, respectively. The solid line at 60°N denotes the North/South boundary. The primary transect lines (NP, MN, SL Lines) for this study are marked. Regions are identified by two letter code as described in the text: North-Outer (NO), North-Middle (NM), North-Inner (NI), South-Outer (SO), South-Middle (SM), and South-Inner (SI). The black arrow denotes the location of sample stations representing the short time-series shown in Fig. 7.

Rates of net primary production (NPP) in the Eastern Bering Sea have been inferred or sparsely measured (in both time and space) for nearly five decades (e.g., Graham and Edwards, 1962; Koblentz-Mishke et al., 1970; McRoy and Goering, 1976; Motoda and Minoda, 1974; Rho and Whitledge, 2007; Saino et al., 1979; Sorokin, 1999). Most daily NPP rates, regardless of season, fall in a relatively narrow range (0.5–0.9 g C m^{-2} d^{-1}; Table 1; Mathis et al., 2010), although much higher rates, up to 13 g C m^{-2} d^{-1} (Niebauer et al., 1995) and with Chl-a concentrations up to 35 μg L^{-1}, can be observed associated with ice-edge diatom blooms. The duration of these ice-edge blooms, outside regions local to moorings, is not well known, and time-series or seasonal measurements, particularly rate measurements, have rarely been conducted to assess the temporal nature of these features (e.g., Niebauer et al., 1995). High summer rates of NPP (up to ~3 g C m^{-2} d^{-1}) have been observed associated with frontal and upwelling regions near the 'Green Belt' (e.g., Sambrotto et al., 2008; Springer et al., 1996), or following storm induced mixing of the water column in shallower regions on the shelf

Table 1
Summary of net primary production and Chl-a standing stocks, and percent of each attributed to large cells, for each region (northern region upper part of table, southern region lower part of table) and domain. Top line in each row is mean ± stdev., and second line (in parentheses) is the range of data.

	Outer Domain		Middle Domain		Inner Domain	
	Spring	Summer	Spring	Summer	Spring	Summer
NPP (g C m^{-2} d^{-1})	0.26 ± 0.18 (0.11–0.46)	–	0.89 ± 1.02 (0.06–2.53)	0.66 ± 0.32 (0.29–0.80)	0.08 ± 0.03 (0.05–0.10)	–
NPP > 5 μm (%)	74.5 ± 32.9	–	47.5 ± 34.9	79.9 ± 18.0	43.1 ± 28.9	–
Chl-a (mg m^{-2})	9.7 ± 4.1 (6.8–12.6)	–	69.5 ± 86.7 (6.5–221.8)	67.5 ± 4.8 (62.9–72.5)	14.1 ± 12.4 (5.3–22.9)	–
Chl-a > 5 μm (%)	67.3 ± 42.0	–	58.9 ± 26.7	77.4 ± 11.3	54.3 ± 0.8	–
n	2	–	5	3	2	–
NPP (g C m^{-2} d^{-1})	3.65 ± 2.70 (0.21–6.65)	1.33 ± 1.18 (0.57–2.96)	0.46 ± 0.51 (0.06–2.20)	1.62 ± 2.17 (0.21–5.35)	0.08	0.27 ± 0.16 (0.16–0.34)
NPP > 5 μm (%)	68.1 ± 28.9	28.4 ± 21.0	76.7 ± 31.4	40.7 ± 27.5	52.8	39.0 ± 16.6
Chl-a (mg m^{-2})	336 ± 270 (12.8–897.1)	35.8 ± 14.8 (24.3–63.9)	40.2 ± 49.6 (4.5–152.8)	24.0 ± 14.9 (8.1–45.7)	5.0	27.3 ± 22.7 (11.3–43.4)
Chl-a > 5 μm (%)	63.4 ± 31.5	18.4 ± 2.8	51.0 ± 24.0	45.8 ± 20.6	35.6	21.9 ± 8.3
n	12	5	11	8	1	2

(e.g., Sambrotto et al., 1986). These observations indicate strong spatial and temporal variability associated with localized areas of high productivity in the Bering Sea. As a result, it is extremely difficult to accurately quantify the magnitude and constrain the uncertainty of shelf-wide, annual productivity. A recent study by Rho and Whitledge (2007) compiled one of the most seasonally and spatially resolved datasets of NPP (based upon ^{13}C-incubations) for the shelf region south of the Pribilof Islands. They estimated annual NPP to be 100–150 g C m^{-2} yr^{-1}, varying with the specific oceanographic domain. Because of the temporal and spatial heterogeneity, the propagated error on individual annual estimates is large, of the order 50–75%. Moreover, Rho and Whitledge (2007) present data from the PROBES program in 1978–1981 and recent data from 1997–1999, with no apparent spring bloom observed in the 1997–1999 data. It is not known whether this is due to spatial sampling discrepancies (i.e., not sampling ice-edge blooms in the later dataset), or to differences in sea ice conditions associated with the different temperature regimes in these two periods (Niebauer et al., 1999). Without continuous, year-round measurements across the entire shelf, an accurate annual shelf NPP value, and therefore changes in NPP induced by ocean warming and subsequent loss of seasonal sea ice, will be difficult, if not impossible, to quantify with certainty (Rho and Whitledge, 2007).

As part of the three year (2008–2010) Bering Sea Ecosystem Study-Bering Sea Integrated Ecosystem Research Program (BEST-BSIERP), a field program was conducted to test the hypothesis that reduced sea ice (due to warmer water temperatures) in the spring resulted in lower spring bloom NPP due to a reduction in Chl-a that is not completely compensated for by increased growth rate at warmer temperatures. The entire three-year field study period however was characterized by lower than average temperatures (Stabeno et al., 2012-a). This study reports spatial and seasonal distributions of NPP during two years, 2008 and 2009, that were colder than any in the prior three decades (Stabeno et al., 2010). Using these data, a vertically generalized productivity model (VGPM) was developed that captured ~83% of the variability in the simulated, in situ NPP rates, and accurately approximated the magnitude of the simulated, in situ NPP measurements. With underway sea surface and meteorological data, this VGPM was used to generate more highly resolved spatial maps of NPP, the first of many steps in determining if seasonal and annual patterns in NPP across the shelf might change in response to climate warming and the loss of seasonal sea ice.

2. Materials and methods

2.1. Sample collection and location

Physical, biogeochemical and biological measurements were made as part of the BEST-BSIERP field campaign on *USCG Healy* cruises to the Eastern Bering Sea in spring 2008 (March 29–May 6; HLY0802), summer 2008 (July 3–30; HLY0803), and spring 2009 (April 3–May 12; HLY0902). The summer 2009 cruise was aboard the R/V *Knorr* (June 14–July 13; KN195-10). CTD stations were generally aligned along three cross-shelf sections that also included stations focused on ice-edge blooms in the spring, and other localized areas of chlorophyll accumulation in the summer (Fig. 1). Process stations were conducted roughly every other day, regardless of position, and included ~24 h simulated, in situ ^{14}C-incubations to determine rates of net primary production (NPP). A total of 15, 10, 19, and 7 process stations were conducted on the four cruises, respectively that spanned the Inner to Outer shelf domains (Fig. 1).

Samples were collected in acid-cleaned 30L Niskin bottles. The CTD package was a SBE 911plus outfitted with the following sensors: SBE-3 temperature sensor, SBE-4 conductivity sensor, SBE-43 dissolved oxygen sensor, Chelsea Aquatrack3 fluorometer and Biospherical QSP2300 photosynthetically active radiation (PAR) sensor that were calibrated prior to each field year. Based upon the PAR profile from the CTD downcast, samples were collected from depths corresponding to ~1.5, ~5, ~9, ~17, ~33, ~55, and ~100% of surface incident PAR (these depths were chosen to match screening in simulated, in situ incubations). At chlorophyll (Chl-a) concentrations less than ~5 μg l^{-1} the depth of the 1% PAR isolume was ~30 m, consistent with prior compilations (e.g., Lorenzen, 1970). The bloom stations where Chl-a exceeded ~5 μg l^{-1} (4 in 2008 and 5 in 2009) were characterized by shallower 1% PAR isolume depths (10–20 m), but the thermal structure of the water column suggested that mixing extending deeper by ~10–15 m (data not shown). For these stations, samples were collected from the mixed layer, but no deeper than 15 m below the euphotic zone, to capture biomass that was mixing through the euphotic zone, and to allow for the vertical separation of the seven Niskin bottle depths. At each process station and light depth a range of discrete phytoplankton-oriented samples were collected including samples for size-fractionated fluorometric Chl-a analysis, picoplankton and nanoplankton abundance and carbon content by quantitative flow cytometry (e.g., Lomas et al., 2010), microplankton abundance and carbon content by inverted microscopy and Utermohl's staining (1958), and size-fractionated HPLC pigment analysis (Lomas et al., 2010); only fluorometric Chl-a data are reported in this study.

For clarity, and consistency with previous work (e.g., Mathis et al., 2010), the entire shelf was divided into six oceanographic domains. Each domain is abbreviated with a two letter code where the first letter is either "N" or "S" to signify the region North or South of 60°N, and the second letter is "I", "M", or "O" for Inner, Middle and Outer domain, respectively, defined by bathymetry (see Introduction).

2.2. Net primary production (NPP)

Rates of NPP were calculated from the autotrophic incorporation of $NaH^{14}CO_3^-$ into particulate organic matter (i.e., particles ≥0.7 μm) using the ratio of added radiocarbon to total inorganic carbon present (based upon salinity; Parsons et al., 1984). Samples were collected from seven discrete light depths into acid cleaned 250 ml square polycarbonate bottles and at each sample depth, ~10 μ Ci of $NaH^{14}CO_3^-$ were added to each of three 'light' bottles, a single 'dark' bottle and a single initial (T_0) bottle. A sample for total added activity was removed from the T_0 bottle at each light depth and immediately added to an equal volume of B-phenylethylamine; variance in total $NaH^{14}CO_3^-$ additions was ≤5% between bottles. Samples were incubated under simulated, in situ conditions (on deck incubators with neutral density screening to mimic collection light depths) for ~24 h. Incubators were fed by surface seawater, although some warming, ~0.5 °C above ambient, was unavoidable. At the end of the incubation, 125 mL sub-samples from each light and dark bottle were filtered through an Ahlstrom 151 (nominal 0.7 μm pore size) and a Whatman Track Etch 5 μm filter and rinsed with 10% HCl to remove residual $NaH^{14}CO_3^-$. Samples were counted on a Perkin Elmer TriCarb 2900LR ca. 48h after the addition of 5 mL of Ultima Gold (Perkin Elmer, USA) scintillation cocktail. Samples were counted for 5 min with the majority of samples having ≤2% counting error. Daily volumetric rates of NPP were calculated from the mean light bottle value corrected for the dark bottle value using the average total added activity for the profile

(Knap et al., 1997). Volumetric rates were integrated to the deepest sample depth (i.e., ~1.5% light level) for total water column NPP. These long incubations likely represent a primary production rate that is closer to net primary production than it is to gross primary production (Marra, 2002) and hence are referred to as NPP.

2.3. Phytoplankton community composition and autotrophic carbon biomass

Samples for pico- and nanoplankton enumeration were collected from the same depths as samples for NPP incubations, fixed with paraformaldehyde (0.5% final concentration), stored at ~4 °C for 1–2 h, before long-term storage at −80 °C. Samples were analyzed on a Becton Dickinson (formerly Cytopeia Inc.) Influx cytometer using a 488 nm blue excitation laser, appropriate Chl-a (692 ± 20 nm) and phycoerythrin (580 ± 15 nm) bandpass filters. The cytometer was calibrated daily with 0.53 μm and 2.88 μm fluorescent microbeads (Spherotech Inc. Libertyville, Illinois, USA). Each sample was run for 4–6 min (~0.2–0.3 mL total volume analyzed), with log-amplified Chl-a and phycoerythrin fluorescence, and forward and right-angle scatter signals recorded. Data files were analyzed from two-dimensional scatter plots based on Chl-a or phycoerythrin fluorescence and characteristic light scattering properties (e.g., DuRand and Olson, 1996) using FCS Express 3.0 (DeNovo Software Inc. Los Angeles, California, USA). Pico-autotrophs were identified as *Synechococcus*-like cells based upon cell size and the presence of phycoerythrin. Nanoeukaryotes were operationally defined as Chl-a containing particles ≥2.88 μm (based upon the mean channel of 2.88 μm beads). This population was further sub-divided into Cryptophyte-like cells (those ≥2.88 μm cells containing phycoerythrin) and other nanoeukaryotes (all other cells ≥2.88 μm cells). Based upon these gating criteria, cells in each identified population were enumerated and converted to cell abundances by the volume-analyzed method (Sieracki et al., 1993). Precision of triplicate samples was <5% for cell concentrations ≥200 cells mL^{-1}. Carbon per cell was estimated for flow cytometrically identified phytoplankton using a calibration curve specific to the flow cytometer used in this study that related cellular particulate organic carbon (POC) to geometric mean cellular forward scatter (proxy for cell size) (e.g., Casey et al., 2011; DuRand et al., 2001). Carbon content of each identified population was estimated by multiplying cell abundance and average POC per cell derived from the calibration curve.

Samples for enumeration of larger microphytoplankton were collected at the same seven depths, and fixed with Alkaline Lugol's (10% w/v, from 1 mL to 200 mL sample) and 1.85% v/v formaldehyde (final concentration), and stored at room temperature until analysis. Ten to 100 mL sub-samples, depending upon Chl-a concentrations, were settled for ~24 h before examination on an inverted microscope (Utermohl, 1958). For each sample, two perpendicular transects through the settled well were counted with cells identified to the lowest possible taxonomic level at 400× magnification. For the most abundant taxa, the total number of cells counted was always >200 cells. For each taxa, up to 25 individual cells were measured and averages taken of the major and minor axis lengths. Cell biovolumes were calculated using the most appropriate geometric shapes as given by Hillebrand et al. (1999) and Vadrucci et al. (2007) and the measured axis lengths. Cell biovolumes were converted to POC per cell using the appropriate carbon/biovolume relationships as given by Menden-Deuer and Lessard (2000). As for the pico- and nano-plankton, population-specific POC was calculated as the product of cell abundance and average POC per cell.

2.4. Chlorophyll a (Chl-a) analysis

At each light depth for each process station, samples (0.1–0.4 L) were gently vacuum filtered (≤5 mm Hg) for total chlorophyll (Chl-a) analysis onto Ahlstrom 151 filters (nominal 0.7 μm pore size) and 5 μm Whatman Track Etch polycarbonate filters under subdued lighting. After filtration, samples were stored frozen at −20 °C until extraction and analysis, which was always within 24 h of collection, and often within 12 h of collection.

For analysis, samples were extracted in 5 ml of 90% acetone for 24 h at −20 °C. Samples were analyzed on a calibrated TD-700 fluorometer with day-to-day performance of the fluorometer tracked using a commercially available solid standard. Day-to-day variability in instrument response was 2–3% depending upon the cruise, with a <2% downward drift in mean readings, perhaps due to lamp output decay, over the duration of any single cruise. This drift appeared constant over each cruise and samples have been linearly corrected based upon the time of sample analysis relative to the beginning of each cruise. Fluorescence readings were taken before and after the addition of 75 μl of 1.2 M HCl and concentrations calculated using standard equations (Parsons et al., 1984).

The underway Chl-a fluorometer data for each cruise were calibrated against discrete near surface Chl-a samples collected by CTD (e.g., Lomas et al., 2009). Briefly, near surface extracted Chl-a concentrations sampled by the current group of researchers (~50 per cruise) were regressed against Chl-a values generated by the fluorometer connected to the underway seawater system (~9 m) from the same station. For each cruise the relationship was very strong, but the regression slope was not always equal to unity. The extracted Chl-a concentrations were assumed to be more accurate and the underway Chl-a data corrected to the extracted Chl-a concentrations using a cruise-specific regression. This calibrated underway dataset was used as one of the input variables to the vertically generalized production model (VGPM, next section) to derive more detailed maps of NPP.

2.5. Calculation of C:Chl-a ratios

Two methods were used to calculate the C:Chl-a ratio. First, the ratio was calculated as the slope of the linear regression between whole community volumetric POC and Chl-a concentrations. POC concentrations were not size-fractionated and therefore this ratio represents the value for the whole community. For the one summer cruise for which bulk POC data are available, bulk POC was plotted against bulk Chl-a for the upper euphotic zone (100-33% PAR) and the lower euphotic zone (33-1% PAR). Second, the ratio was estimated as the quotient of autotrophic cell carbon derived from cell biovolume vs. carbon relationships and Chl-a concentrations. For the latter, ratios were estimated for autotrophs ≥5 μm (based upon length estimates from inverted microscopy) as well as for autotrophs <5 μm (including data for pico- and nanoplankton). Values were binned by collection depth (i.e., the upper, 100-33%, and lower, 33-1%, euphotic zone), bloom status (i.e., total Chl-a greater than or less than 1 μg l^{-1}), size fraction and nutrient availability (i.e., high and low NO_3^- concentrations) as all of these are known to impact C:Chl-a ratios.

2.6. VGPM model

A map of euphotic zone integrated NPP on the Eastern Bering Sea shelf was obtained using a vertically generalized productivity model (VGPM; Behrenfeld and Falkowski, 1997). The VGPM requires as input variables: surface Chl-a concentrations (C_{surf}; mg m^{-3}), daily PAR flux (E_o; μmol photons m^{-2} d^{-1}), daylength (DL; h), an estimate of the euphotic zone depth (Z_{eu}; m), and an

estimate of the optimum biomass-specific photosynthesis rate (P_b^{opt}; mg C mg Chl-a^{-1} h^{-1}; Eq. (1))

$$\int \mathrm{NPP}_{VGPM} = C_{surf} \times Z_{eu} \times P_{opt}^{b} \times \mathrm{DL} \times \left[\frac{0.66125 \times E_o}{E_o + 4.1}\right] \quad (1)$$

Discrete surface Chl-a values (see above), from each process station were used when directly comparing the model output to the measured in situ NPP at each process station. Incoming daily PAR flux and daylength for the ~24 h period of the ^{14}C NPP incubations were determined from the shipboard meteorological sensors mounted on a mast at the bow, ~5–10 m above the sea surface. On cruise KN-195, short wave radiation (SWR; J m^{-2} s^{-1}) rather than PAR was measured and these values were converted to PAR (μmol photons m^{-2} s^{-1}) by dividing by 0.225 J μmol^{-1} (Siegel and Dickey, 1987). All PAR and SWR sensors were calibrated prior to each cruise year and it was assumed that the calibration was valid for the duration of each cruise year. PAR (both directly measured and converted from SWR) readings were recorded every minute and a value of three times the nighttime sensor reading (~5 μmol photons m^{-2} s^{-1}) was used as the threshold to mark the portion of a given 24 h day where light intensity was sufficient for NPP to be positive (i.e., daylength). This value is in part arbitrary as there is no direct data for the Eastern Bering Sea that could be found (or was measured by the researchers on this manuscript) to better define this threshold, but it is reasonable based upon personal experience in other systems. Using this threshold to define the daylength, the daily light dose (units of mol photons m^{-2}) was integrated. At each process station the 1% PAR depth was directly measured from the CTD PAR sensor, and this value was used in comparing the model output to measured NPP data at process stations. Previously, P_b^{opt} has been derived solely as a function of global sea surface temperature for global satellite productivity models (see Behrenfeld and Falkowski, 1997 for justification). Using productivity and sea surface temperature measurements (T) from this dataset an equation was derived specific for this dataset (Fig. 2 and Eq. (2)) and was used in the model calculations

$$P_{opt}^{b} = -0.041 \times T^3 + 0.293 \times T^2 + 0.262 \times T + 0.617 \quad (2)$$

The equation was similar to Behrenfeld and Falkowski, (1997; dashed line in Fig. 2) but the main difference was higher P_{opt}^{b} (mg C mg Chl-a^{-1} h^{-1}) values in the 5–7 °C range in this study. Interestingly the decrease in P_{opt}^{b}(mg C mg Chl-a^{-1} h^{-1}) in the 8 °C bin that was observed by Behrenfeld and Falkowski (1997) was also observed in this dataset. For temperate and sub-Arctic regions, where there is expected to be large spatial/seasonal oscillations in primary production and the mean autotrophic cell size, it has been suggested that a modified P_{opt}^{b} formulation, based upon temperature and Chl-a, be used that accounts for the general observation that at high Chl-a concentrations, large cells with lower specific P_{opt}^{b} values are dominant (Kameda and Ishizaka, 2005; their Eq. (9)). Note that this model might not be applicable to the oligotrophic ocean (e.g., Fernandez et al., 2003). Both approximations of P_{opt}^{b} were used and it was found that the approximation factoring changes in Chl-a rather than temperature alone performed better. For each process station on the four cruises (51 total stations) the VGPM model was used to calculate NPP using the above described inputs.

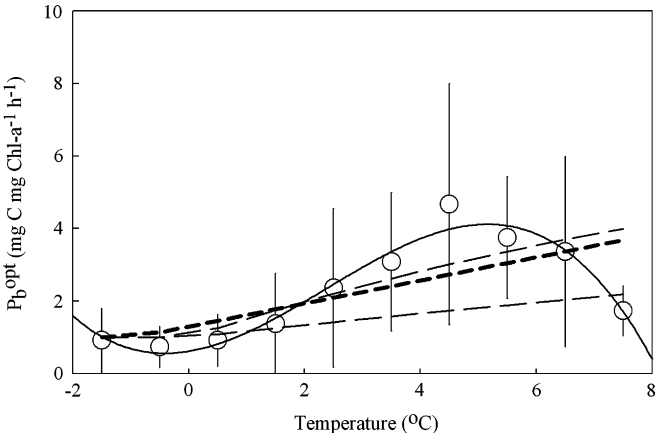

Fig. 2. Average temperature response of P_b^{opt} (mg C mg Chl-a^{-1} h^{-1}) for all process stations (n=51) divided into 0.5 °C bins. The average error of temperature measurements was < 0.1 °C. The solid line is the 3rd-order polynomial fit to the data (Eq. (2)). The heavy short dashed line is the temperature vs. P_b^{opt} (mg C mg Chl-a^{-1} h^{-1}) relationship from Behrenfeld and Falkowski (1997) for this temperature range. The thin long dashed lines are the temperature vs. P_b^{opt} (mg C mg Chl-a^{-1} h^{-1}) relationships from Kameda and Ishizaka (2005) for Chl-a values of 0.25 mg m^{-3} (upper thin long dashed line) and 20 mg m^{-3} (lower thin long dashed line).

The temperature-dependent P_{opt}^{b} was then used with underway data and the VGPM to generate a more spatially resolved map of calculated NPP. As an example, data for HLY0902 and KN195 are presented. For the duration of each cruise, the underway surface Chl-a data, PAR flux and daylength were determined as above. Euphotic zone depth was estimated from the linear relationship between the natural log of the measured euphotic zone depth and the natural log of the discrete surface Chl-a concentrations (e.g., Lorenzen, 1970). P_{opt}^{b} was estimated as above using underway measured sea surface temperature and Chl-a. Using continuous (1 min averaged) underway Chl-a and sea surface temperature data can provide a continuous calculation of NPP. However, because it was daily NPP that the VGPM was validated upon for this region, the continuous record was segmented into 24 h units, starting at 0500 local time each day to capture the entire solar day. Mean values of Chl-a, in situ sea surface temperature, and the PAR flux and daylength over each segment were used as described above to calculate euphotic zone integrated NPP. The central latitude/longitude position within each 24 h period was used to georeference these rates of euphotic zone integrated primary production into one of the six (6) geographical regions on the Bering Sea shelf (Fig. 1). The range for each 24 h period varied depending upon science activities and the data are not weighted for these differences. The result is a calculation of daily NPP for each day at sea; for 2009 this would roughly triple the number of data points used in regional estimates.

3. Results

3.1. Environmental conditions during cruises

While many of the process stations were on cross-shelf sections, others were dispersed to capture spatially variable features (e.g., ice-edge blooms). The result was a set of euphotic zone NPP estimates and Chl-a concentrations that spanned the Inner, Middle and Outer shelf domains in both the Northern and Southern region (Fig. 1). Both 2008 and 2009 were characterized as 'cold years' relative to the long-term observational mean at mooring station M2 (56° 36′N 164° 37′W), with greater seasonal sea ice extent and a larger cold pool (Stabeno et al., 2012-b). Due to these similarities between years, data are presented as a 'cold-year composite' view of NPP and Chl-a on the Eastern Bering Sea shelf.

3.2. Variability of measured integrated rates of NPP and Chl-a standing stocks

Measured euphotic zone integrated (g C m^{-2} d^{-1}) rates of NPP showed substantial variability across the shelf domains in both seasons ranging from a low of 0.08 to a high 6.65 g C m^{-2} d^{-1} (Fig. 3, Table 1), but are within the range of previously published

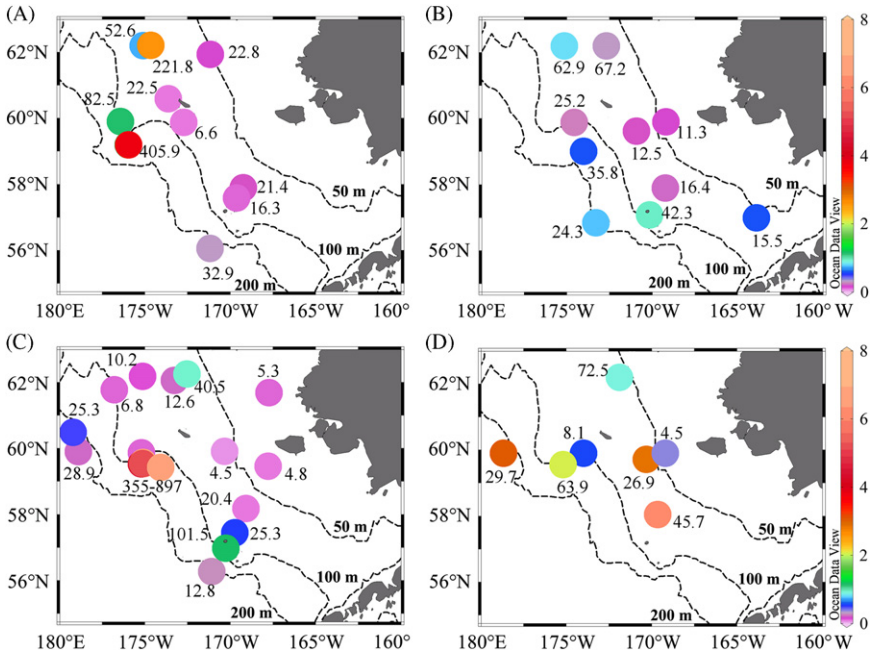

Fig. 3. Surface euphotic zone integrated primary production (g C m^{-2} d^{-1}) measured for each cruise; (A) Spring 2008, (B) Summer 2008, (C) Spring 2009, and (D) Summer 2009. The number associated with each dot is euphotic zone integrated Chl-a (mg Chl-a m^{-2}).

Table 2
Selected summary of average daily NPP data all determined by ^{14}C-incubations except Rho and Whitledge, 2007 who used ^{13}C-incubations. Season refers to the time period of sampling included in determining the average daily values presented (e.g., annual means that data collected throughout the year were used in calculating the average value presented).

Region/domain	Season	NPP (g C m^{-2} d^{-1})	Reference
Northern region	Spring	4.1	McRoy et al. (1972)
Northern region	Spring	0.05–2.53	This study
Northern region	Summer	0.29–0.8	This study
Southern region	Spring-Summer	0.24	McRoy et al. (1972)
Southern region	Spring	0.06–6.65	This study
Southern region	Summer	0.16–5.35	This study
Outer Domain	Annual	0.63	Tsiban and Korsak (1987)
Outer Domain	Annual	1.4	Sorokin (1999)
Outer Domain	Annual	0.40	Rho and Whitledge (2007)
Middle Domain	Annual	2.2	Sorokin (1999)
Middle Domain	Annual	0.41	Rho and Whitledge (2007)
Inner Domain	Annual	0.34	Rho and Whitledge (2007)
Total Bering Sea	Annual	0.92	Taguchi (1972)
Total Bering Sea	Annual	0.80	McRoy and Goering (1976)
Total Bering Sea	Annual	0.50	Motoda and Minoda (1974)
Total Bering Sea	Annual	0–4.1	Saino et al. (1979)

data (Table 2). Despite the high variability, this dataset shows some domains have generally higher/lower NPP during the spring and summer season, and that within a domain there can also be significant variability. During spring, the lowest NPP rates generally were in the inner domain with values ~0.1 g C m^{-2} d^{-1}, although it is important to point out that there are only two sample stations in the NI domain, and one in the SI domain (Table 1). These low NPP rates were also associated with some of the lowest integrated Chl-a standing stocks observed (5–14.1 mg Chl-a m^{-2}; Table 1) which is likely due to light limitation under the extensive ice cover. Within the middle domain, NPP rates were higher and more variable, to the north (0.89 ± 1.02 g C m^{-2} d^{-1}; Fig. 2A and C) due to the influence of the open water of the St. Lawrence Island Polyna that allowed for higher biological activity. In the SM domain, rates were on average lower and as variable (0.46 ± 0.51 g C m^{-2} d^{-1}) as this region was still largely covered with seasonal sea-ice at the time of sampling. In the SO domain, production rates were highest (3.65 ± 2.70 g C m^{-2} d^{-1}), due to the intense ice-edge blooms that occurred in this domain in the spring (Fig. 3C, see also Stabeno et al., 2012-b). In one of the ice-edge blooms sampled in 2009, observed daily production rates reached a maximum of 6.65 g C m^{-2} d^{-1}; or about one-half the previously recorded maximum values for ice edge blooms in this region (~13 g C m^{-2} d^{-1}; Niebauer et al., 1995). With the exception of the NO domain, Chl-a standing stocks in the Middle and Outer domains were from 2 to 20-fold higher than in the Inner domain (Table 1).

During summer, no process stations were sampled in the NO or NI domains. In the SI domain NPP rates were higher (0.27 ± 0.16 g C m^{-2} d^{-1}; $n=2$), than in spring, though still substantially lower than summer rates in the other domains. NPP

rates in the SM and SO domains were >1 g C m^{-2} d^{-1}, though not as high as the spring-bloom rates in the SO domain. Thus, regardless of season, NPP generally increased from inshore to offshore in the southern region. Unlike the spring, where the cross-shelf gradient in NPP was closely linked to a cross-shelf gradient in Chl-a, during summer, cross-shelf gradients in Chl-a in the southern region were not as distinct. Chl-a standing stocks were 27.3 ± 22.7, 24.0 ± 14.9, and 35.8 ± 14.8 mg Chl-a m^{-2} in the SI, SM, and SO domains, respectively, during summer.

Vertical sections of NPP and Chl-a across the shelf in spring show highest values in surface waters that decreased with depth down to ~40 m (near the dataset average euphotic zone depth; Figs. 4–6). Consistent with the spatial patterns above, volumetric NPP and Chl-a increased from the southern region (NP Line,

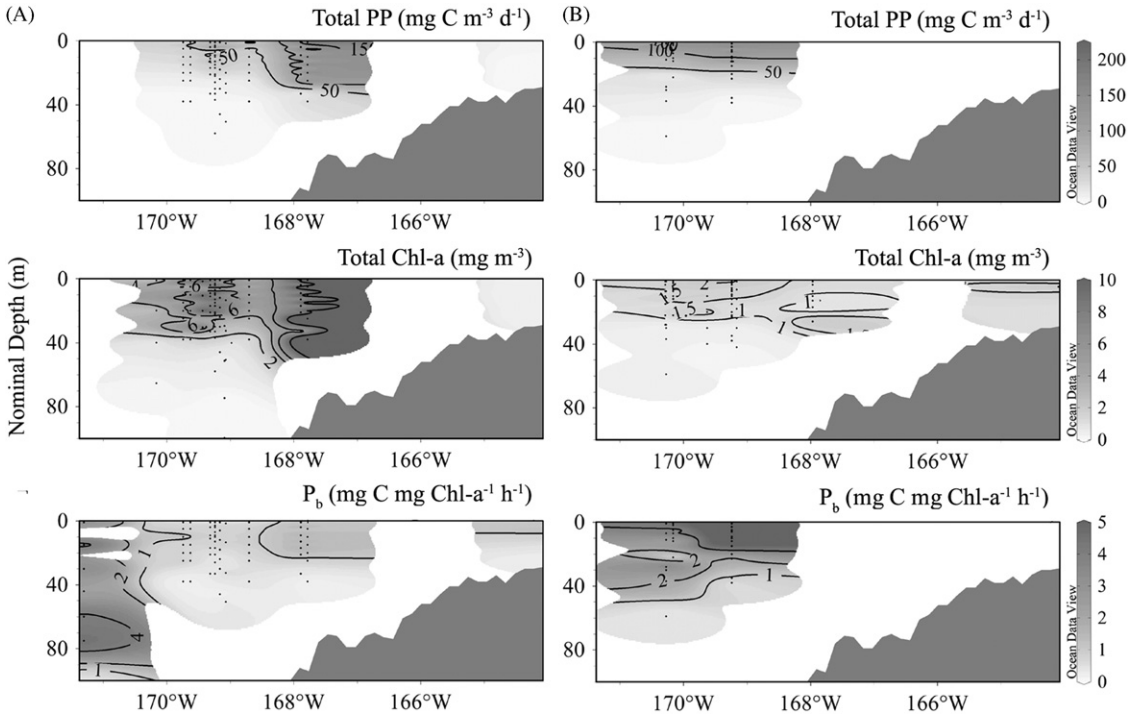

Fig. 4. Composite vertical sections of total NPP (top; mg C m^{-3} d^{-1}), total Chl-a (middle; mg Chl-a m^{-3}) and biomass-specific productivity (bottom; mg C mg Chl-a^{-1} h^{-1}) for the NP Line during spring (left) and summer (right). Filled contours are for the same range between panels of the same parameter, but specific contour lines differ. Scale bar on the right applies to both panels in the same row. Small dots represent stations/depths where data were collected.

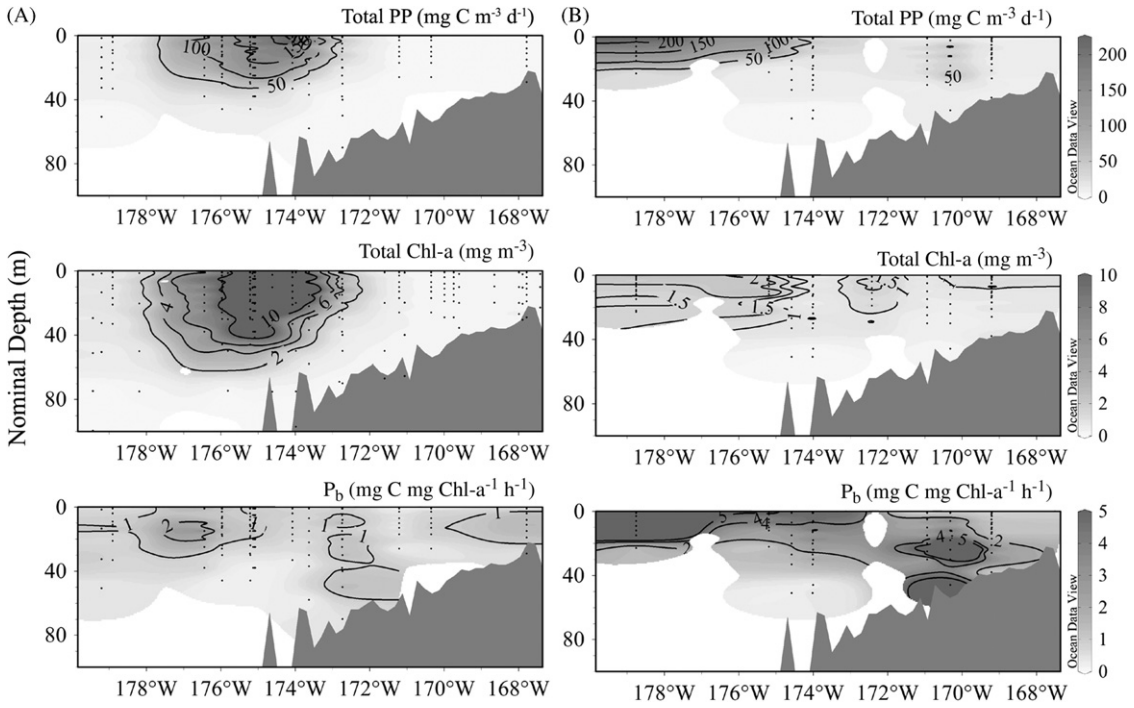

Fig. 5. Same as Fig. 4 except plots are for the transition zone between southern and northern domains (MN Line).

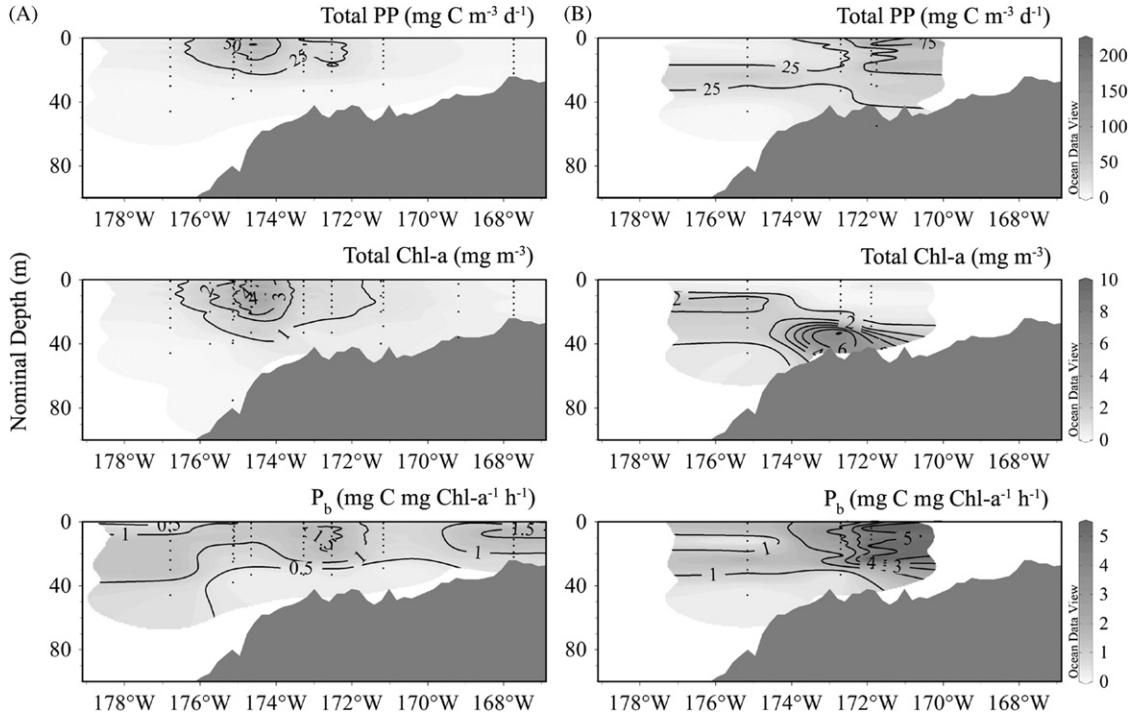

Fig. 6. Same as Fig. 4 except plots are for the SL Line. (A) SL line, Spring and (B) SL line, Summer.

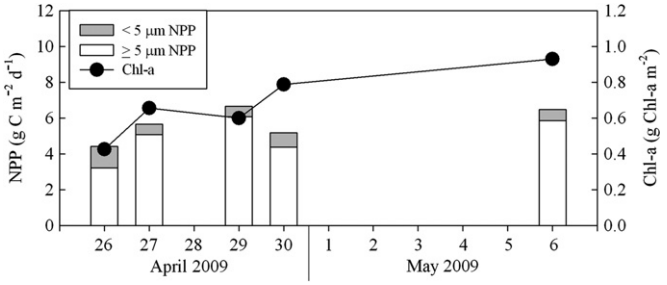

Fig. 7. Time-series of ice-edge bloom euphotic zone integrated primary production (bars; g C m^{-2} d^{-1}) and Chl-a concentrations (line; mg m^{-2}). Each day was a separate, single station, but all stations were within a 16 km radius.

open water at the time of sampling, Fig. 4), was maximal at the transition region (~60°N, MN Line, near the receding ice edge at the time of sampling, Fig. 5), and then decreased further north (SL Line, under ice at the time of sampling, Fig. 6). During spring, regardless of latitude, the highest local NPP and Chl-a values were geographically linked to the frontal region near the 100 m isobath that separates the Middle and Outer domains, but were broader than the frontal region itself. Ice-edge blooms occurred in the NO/SO transition region where ice-retreat was actively occurring at the time (Fig. 5). In these ice-edge blooms, volumetric NPP exceeded 150 mg C m^{-3} d^{-1} and in the larger bloom studied in 2009, Chl-a accumulated over the repeated sampling to ~35 mg m^{-3} (Fig. 7). Because of the covariance of NPP and Chl-a, there were no clear patterns in biomass-specific productivity (P_b). P_b values were ~1–2 mg C mg Chl-a^{-1} h^{-1} over most of the shelf regardless of domain or region, although values tended to be higher near biomass maxima, presumably as these populations were more actively growing, and off the southern shelf in slightly warmer water (e.g., Fig. 4).

In summer, in the southern and transition regions of the shelf, highest volumetric NPP rates were still observed in the near surface waters, but were higher than in spring (Table 1), and spanned the entire SO domain from the 100 m isobath seaward to the end of the station grid (Figs. 4, 5). Chl-a biomass was generally elevated in the surface waters in the SO domain relative to SM and SI domains. Chl-a, like NPP, was similarly dispersed over the Outer domain and with no large coherent blooms, as was observed in the spring. The NM domain, the only region for which there is summer data, was similar to the spring, with elevated volumetric NPP rates in the surface waters, but maximum rates had shifted landward to the NM/NO domain interface (Fig. 6). While elevated Chl-a concentrations were still present in surface waters, the most striking feature was a very high Chl-a peak, with values of >6 mg m^{-3}, near the benthos at the NM/NI domain (Fig. 6). Given the relatively shallow water depth in this region, it is not clear whether this Chl-a maximum represented growth of a resident low-light population near the seafloor, or tidal resuspension of previously settled material (Moran et al., 2012). P_b values tended to be substantially higher in summer than in spring regardless of domain or region (Figs. 4–6).

3.3. Variability in the carbon to chlorophyll (C:Chl-a) ratio

The C:Chl-a ratio is known to vary primarily as a function of mean cell size, light history, and nutrient status (e.g., Geider, 1987; Malone, 1980). The shelf-wide C:Chl-a ratio, calculated using biovolume to carbon conversions, was 50 ± 20 ($n=109$) in spring and 55 ± 14 ($n=89$) in summer. When parsed into upper (100-33% PAR) and lower (33-1% PAR) portions of the euphotic zone, bloom status (i.e., Chl-a >1 μg l^{-1} in a given size fraction), and cell size, average values generally changed in the direction expected although the differences were not statistically significant (Table 3). For example, when Chl-a was <1 μg l^{-1} (non-bloom condition), cells <5 μm had a C:Chl-a of 57 ± 18 and 59 ± 18 in upper and lower euphotic zones, respectively, whereas cells ≥ 5 μm had C:Chl-a ratios of 51 ± 14 and 51 ± 19, respectively (Table 3). Under bloom conditions, average C:Chl-a ratios for each sample depth and cell size bin were on average lower by only 5–25%. In summer, the same pattern held for non-bloom conditions. C:Chl-a ratios in cells <5 μm (56 ± 14 and 54 ± 15) were

Table 3
Summary of C:Chl-a (average ± stdev.) ratio data from the Eastern Bering Sea during 2008 and 2009. Within each season, data are subdivided by light depth (100–33% PAR and 33–1% PAR), bloom status (yes/no; bloom is defined as $>1\ \mu g\ L^{-1}$ in a given size fraction), autotrophic particle size fraction ($>5\ \mu m$ and $<5\ \mu m$), and ratio calculation method. This division was done to highlight potential differences in the C:Chl-a ratio due to nutrient status, light history, autotrophic growth state, and taxonomic shift; all parameters known to have an impact on the C:Chl-a ratio. See text for details on calculations. For 'correlation' calculations r is the Pearson correlation coefficient, and in all calculations, n is the number of data pairs used. n.d. is no data.

Depth	Bloom (Y/N)	Size fraction (μm)	Method	POC (mg C m^{-3})	Chl-a (mg m^{-3})	POC:Chl-a
Spring cruises						
100-33% PAR	N	>5	Biovolume—C	3.3 ± 2.4	0.07 ± 0.05	51 ± 14 (n=10)
		<5	Biovolume—C	12.6 ± 7.9	0.25 ± 0.16	57 ± 18 (n=14)
	Y	>5	Biovolume—C	227 ± 232	5.4 ± 5.3	42 ± 3 (n=12)
		<5	Biovolume—C	68.5 ± 62.1	1.8 ± 1.6	42 ± 16 (n=24)
33-1% PAR	N	>5	Biovolume—C	3.9 ± 3.2	0.08 ± 0.07	51 ± 19 (n=11)
		<5	Biovolume—C	12.2 ± 6.8	0.23 ± 0.10	59 ± 18 (n=20)
	Y	>5	Biovolume—C	134 ± 204	3.0 ± 4.1	45 ± 6 (n=11)
		<5	Biovolume—C	78.8 ± 72.1	1.8 ± 1.6	56 ± 13 (n=23)
Summer cruises						
100-33% PAR	N	>5	Biovolume—C	7.9 ± 3.2	0.16 ± 0.04	49 ± 9 (n=4)
		<5	Biovolume—C	16.8 ± 11.6	0.32 ± 0.25	56 ± 14 (n=30)
	Y	>5	Biovolume—C	12.8 ± 12.9	0.27 ± 0.28	48 ± 5 (n=10)
		<5	n.d.	n.d.	n.d.	n.d.
33-1% PAR	N	>5	Biovolume—C	60.3 ± 15.1	1.66 ± 0.32	36 ± 5 (n=4)
		<5	Biovolume—C	22.8 ± 24.2	0.46 ± 0.42	54 ± 15 (n=44)
	Y	>5	Biovolume—C	117 ± 154	3.23 ± 4.4	45 ± 13 (n=4)
		<5	n.d.	n.d.	n.d.	n.d.
100-33% PAR	N	19 ± 9% > 5	Correlation	n.d.	n.d.	110 ± 22 (r=0.72) (n=24)
33-1% PAR	N	19 ± 10% > 5	Correlation	n.d.	n.d.	117 ± 10 (r=0.95) (n=18)

on average higher than that for cells $\geq 5\ \mu m$ (49 ± 9, and 36 ± 5) regardless of whether they were found in the upper or lower euphotic zone (Table 3). The same comparison cannot be made for summer bloom conditions as Chl-a in the $<5\ \mu m$ fraction never exceeded $1\ \mu g\ l^{-1}$.

These ratios calculated from biovolume to carbon conversions are a factor of two lower than the summer C:Chl-a ratio derived from the linear correlation slope (110 ± 18 g C:g Chl-a for the upper euphotic zone and 117 ± 10 g C:g Chl-a for the lower euphotic zone; Table 3). For the subset of stations where large-cells dominated the total Chl-a, the linear regression slope resulted in a statistically identical value to the total dataset.

3.4. Time-series of NPP and Chl-a standing stocks in an ice-edge bloom

During spring 2009, an intense ice-edge bloom was sampled repeatedly to generate a short time-series of observations (Fig. 7 and station location shown by the arrow in Fig. 1). The ice-edge bloom had apparently already begun by the first sample time point as euphotic zone integrated NPP was ~4 g C m^{-2} d^{-1} and increased to a maximum of ~6.5 g C m^{-2} d^{-1} by the end of the short time-series. The euphotic zone integrated NPP rates in this ice-edge bloom were the highest observed at any of the stations of the four cruises, and were at the high end of average daily areal rates in other Eastern Bering Sea studies (Table 2). Time-integrated NPP was ~55 g C m^{-2} (assuming rates on 30th April remained at that level until the next measurement 6th of May). During this 10-day period Chl-a concentrations increased from ~10 mg m^{-3} to ~35 mg m^{-3}, or a euphotic zone integrated Chl-a standing stock of ~1 g m^{-2}.

3.5. Comparison of the VGPM to incubation-based NPP

Due to the high tidal and wind mixing over much of the study region and seasons, a significant relationship (R^2=0.58, N=51, $P<0.001$) existed between surface Chl-a and euphotic zone integrated Chl-a (Fig. 8A). Despite the wide range in magnitude due to seasonal differences in temperature and biomass size-structure, biomass-specific productivity profiles were generally uniform down to the lowest light level sampled (~1.5% PAR) where they decreased (Fig. 8B). This was primarily due to sharp reductions in NPP values at the lowest light level.

NPP rates for process stations estimated from the VGPM compared well with the incubation-based ^{14}C NPP measurements, regardless of the P_b^{opt} parameterization (Fig. 9). Using a P_b^{opt} parameterization solely defined by temperature, the VGPM successfully captured ~75% of the variability in measured NPP (Fig. 9A). The overall model accuracy for this P_b^{opt} parameterization was 0.85 ± 0.07 (Model II regression slope of VGPM calculated vs. measured NPP), but was less accurate at the high (>1 g C m^{-2} d^{-1}) productivity stations associated with the ice-edge blooms where the model substantially underestimated measured NPP. These high productivity stations tend to be dominated by blooms of large diatoms. The P_b^{opt} parameterization that accounts for both temperature and total Chl-a (Fig. 9B) captured a similar amount of variability, ~83%, in measured NPP but was more accurate (0.92 ± 0.06, Model II regression slope of VGPM calculated vs. measured NPP) as a result of a better model estimation at the high productivity stations. The VGPM model residuals were plotted against measured NPP and no readily obvious or statistical trend was observed (Fig. 9C). One outlier from KN-195 was removed (Dixon's Q-test, Q_{test}=0.273, $Q_{c,95\%}$=0.19) where the VGPM result was ~80% greater than the measured value. This value appears to be an outlier although it cannot be determined if it is due to a lower estimated P_b^{opt} or a measured productivity (6.8 g C m^{-2} d^{-1}) that is exceptionally high for the relatively low concentration of Chl-a (1.15 mg Chl-a m^{-3}). The mismatch (~10%) between the magnitudes of the model output and the measured NPP is likely due to the accumulation of small errors in several parameters as the major assumptions (uniformity of P_b^{opt} with depth and statistical relationship between surface Chl-a and euphotic zone integrated Chl-a) are well validated, and all sensors used to collect input data

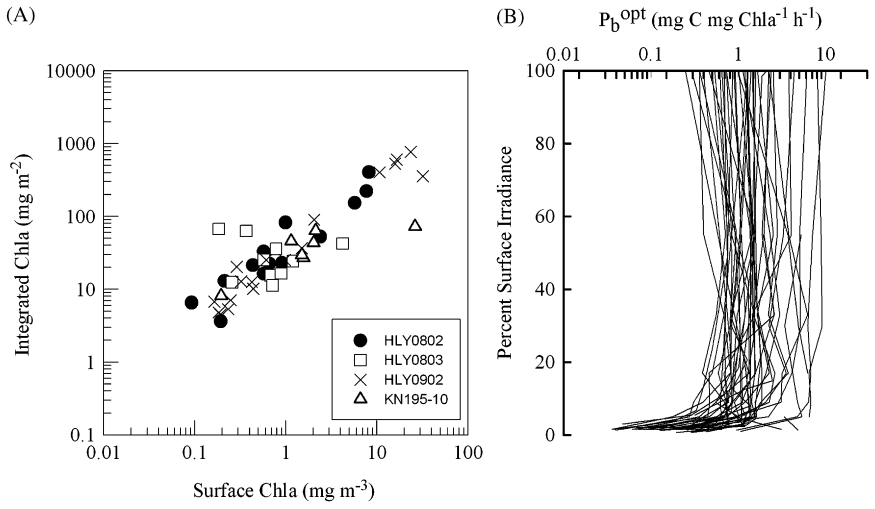

Fig. 8. (A) Euphotic zone integrated Chl-a (mg m^{-2}) vs. surface Chl-a concentrations (mg m^{-3}) by cruise. (B) Profiles of biomass-normalized productivity (P_b; mg C mg Chl-a^{-1} h^{-1}) as a function of percent surface irradiance from all process stations presented in this analysis.

(PAR sensor, thermosalinograph and Chl-a fluorometer) were routinely calibrated before each cruise.

4. Discussion

4.1. Controls on daily NPP and growth

Daily NPP rates measured on the Eastern Bering Sea shelf in the cold years of 2008 and 2009 (Table 1) were comparable to previous estimates of daily NPP (Table 2). These previously published daily NPP rates are the average values (or range in some cases) of all data collected over a season or the entire annual growing period as presented by the original authors. Our data (e.g., Fig. 3) highlight the importance of localized enhancements of NPP such as ice-edge blooms where production can exceed observed regional and/or seasonal average values, and their contributions to annual system productivity (discussed below).

Primary production on the southern middle and outer Bering Sea shelf domains is generally regarded as transitioning seasonally from light limitation in the winter, when sea-ice extent is maximal, to nutrient (primarily nitrogen) limitation in the summer as NO_3^- concentrations are reduced to near zero, while PO_4^- concentrations remain detectable. During the summer season, much of the NPP on the shelf is supported by rapid regeneration of inorganic nutrients (e.g., NH_4^+) and as a result is commonly lower than during the spring (e.g., Hansell et al., 1989). Storm induced vertical mixing and nutrient entrainment into the euphotic zone can lead to localized enhancement of NPP to values similar to those found in spring blooms; this results in significant spatial and interannual variability during the summer (e.g., Sambrotto et al., 1986).

Recent evidence however, suggests that during winter/spring in the southern outer domain (but more generally areas in the southern domain less influenced by seasonal sea ice) there may be insufficient iron to support the seasonal drawdown of NO_3^- (Aguilar-Islas et al., 2008). Considering the importance of iron in the synthesis of important cellular enzymes, namely photosynthetic enzymes, iron limitation may be synergistic with light limitation during the winter/spring period in this domain which would be difficult to assess without direct bioassay experiments. Iron concentrations in sea ice are elevated, though quite variable. The retreat of sea ice edge has been hypothesized to release this iron into surface waters. As a result, northern shelf domains, that are more consistently within the influence of seasonal sea ice (Stabeno et al., 2010) have been shown to have sufficient iron to stimulate the complete drawdown of NO_3^- by large diatoms. Owing to the variability of iron in the sea ice, climate change impacts on sea ice extent and/or duration may have a substantial impact on the magnitude and spatial extent of the Eastern Bering Sea spring bloom.

Associated with the seasonal drawdown in nutrients is a seasonal shift in the distribution of autotrophic cell sizes, from cells ≥ 5 μm dominating in the spring (diatoms and dinoflagellates) to cells <5 μm dominating in the summer (generally flagellates; Moran et al., 2012). Exceptions are storm-derived mixing events in summer that induce diatom blooms. In many other systems this shift in phytoplankton cell size to smaller cells is in response to lower macronutrient nutrient concentrations, where smaller cells compete more successfully for limiting nutrients (e.g., Malone, 1980). In general, the reduction in cell size and nutrients results in reductions in both the variability (i.e., presence/absence of localized areas of enhanced primary production) and the magnitude of primary production (e.g., Sprules and Munawar, 1986).

Distributions of size-fractionated NPP and Chl-a from these cruises yield several important observations regarding phytoplankton growth rate. First, on average, spring Chl-a biomass is dominated by large (≥ 5 μm) cells, though there were stations from all three domains indicating Chl-a biomass dominated by small (<5 μm) cells (Fig. 10A), particularly when the integrated Chl-a biomass was low in ice-covered northern regions. The opposite scenario was observed during the summer (Fig. 10B). Second, in spring, and with the exception of a few outlying data points, there was a roughly 1:1 correspondence between the contributions of large cells to NPP and Chl-a biomass, regardless of their absolute activity and abundance. The implication is that, on average, the carbon to Chl-a ratio (C:Chl-a) is likely to be similar across cells of different sizes (discussed in detail below; Table 3); this observation has also been reported from a number of other marine ecosystems (e.g., Maranon et al., 2001; Tamigneaux et al., 1999; Tremblay and Legendre, 1994). Third, primary production is related to Chl-a biomass via the growth rate of primary producers and the cellular C:Chl-a ratio. Given that C:Chl-a ratios are not statistically different between size classes and that in spring there is a reasonable 1:1 correspondence of contributions to production and Chl-a, these data suggest that on average all cells, regardless of size, are growing at roughly similar rates during the spring.

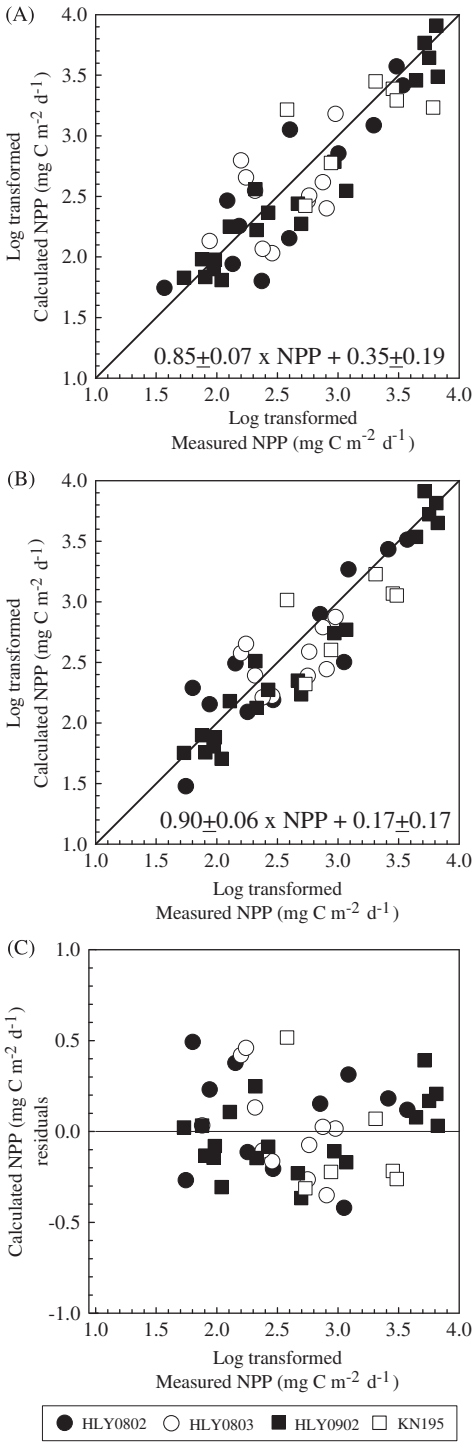

Fig. 9. Log-transformed NPP using the VGPM vs. measured NPP from ^{14}C-incubations. (A) Model using P_b^{opt} parameterization solely dependent upon sea surface temperature. Pearson correlation (r=0.89); least squares fit: Calc. NPP=0.85 ± 0.07 × Meas. NPP+0.35 ± 0.19, $P<0.001$ for slope; normal data distribution assumption, P=0.556; constant variance assumption, P=0.99. (B) Model using P_b^{opt} parameterization dependent upon sea surface temperature and Chl-a using equations of Kameda and Ishizaka (2005). Pearson correlation (r=0.91); least squares fit: Calc. NPP=0.90 ± 0.06 × Meas. NPP+0.17 ± 0.17, $P<0.001$ for slope; normal data distribution assumption, P=0.156; constant variance assumption, P=0.82. (C) Calculated NPP residuals (using the sea surface temperature and Chl-a P_b^{opt} parameterization) plotted against log-transformed measured NPP.

Phytoplankton growth rates can be estimated from the biomass-specific production rate (g C g Chl-a^{-1} d^{-1}) and the C:Chl-a ratio of the same sized particles. Estimates of C:Chl-a ratios using biovolume to carbon conversions averaged ~50 regardless of sampling depth, cell size or nutrient status. Although average values did vary in a manner consistent with expectations, the differences were not statistically significant due to the high variability among samples. C:Chl-a ratios generally increase as a function of cell size (e.g., Malone, 1980) due to a reduction in the package effect, and as a function of nitrogen limitation due to reduced ability to synthesize nitrogen-rich Chl-a (Stramski et al., 2002). The relative differences between small and large cell C:Chl-a ratios were similar whether it was spring (nitrogen-replete) or summer (nitrogen-deplete). The most likely explanation for this observation is that during the summer NO_3^- concentrations were low, relative to spring, but not always to below the method detection limit. In addition, other nitrogenous substrates (e.g., NO_2^- and NO_4^+) were present in detectable concentrations suggesting that the cells in summer were not as nitrogen-limited as one might expect (e.g., Mordy et al., 2010, 2008). Indeed, euphotic zone total inorganic nitrogen concentrations ranged from ~0.1 to 15 μmol L^{-1} during the summer, with the majority of data falling between ~2–15 μmol L^{-1} (data not shown). Using the slope of the correlation between bulk POC and Chl-a resulted in a statistically higher C:Chl-a ratio (Table 3). This was not due to the inclusion of inorganic carbonates in particulate carbon analysis as samples are always fumed with concentrated HCl to remove carbonates (Knap et al., 1997). One possible explanation for the higher ratios via linear regression may be the covariation of another particulate carbon pool that does not contain Chl-a, such as bacterial biomass, but would also be retained on nominal pore size 0.7 μm glass fiber filters. Bacterial abundance generally follows phytoplankton abundance (although explicit data for this study do not exist) and a variable, but high fraction (often > 50%), of bacteria in oceanic and coastal systems are retained on GF/F filters as used here (Bradley et al., 2010; Lee and Fuhrman, 1987). It is a reasonable assumption that at higher Chl-a concentrations more bacterial biomass would be retained on the filter than at low Chl-a. As a result, bacterial biomass might be expected to impact the slope of the correlation (i.e., the C:Chl-a) more than the intercept (the non-pigmented particulate carbon). However, due to a lack of data this is speculation. Interestingly, Guo et al. (2004) using similar methods to our correlation approach in the Arctic reported a C:Chl-a ratio of 70, which is much higher than the ratio of ~30 found by Sherr et al. (2003) and Campbell et al. (2009) also in the Arctic using a biovolume to carbon conversion approach. This suggests that there may be something fundamentally different between these two approaches to calculate the C:Chl-a ratio. For the remainder of this paper, the C:Chl-a ratios based upon biovolume to carbon conversions only are used.

Using the average seasonal C:Chl-a value and the data compiled in Table 1, the average growth rates across all regions in the spring span a relatively narrow range, 0.11 to 0.35 d^{-1} (avg ± stdev., 0.22 ± 0.09 d^{-1}). In contrast, growth rates in the summer averaged over all domains were twice as high as in the spring (0.42 ± 0.17 d^{-1}, Mann–Whitney Rank Sum test, $P<0.001$), implying a more physiologically active population likely due to the seasonal alleviation of light (and perhaps temperature) limitation. Moreover, this supports the early contention that summer phytoplankton populations were not strongly nitrogen-limited during these cruises. Specifically, larger cells in summer 2009 appear to be responsible for these enhanced average growth rates. Data from summer 2009 (Fig. 10B) indicate that larger cells contribute more to NPP than to Chl-a (values consistently above the 1:1 line), despite similar average C:Chl-a ratios (see above), and therefore were growing faster than co-occurring small cells. Interestingly, Shiomoto et al. (1997) observed statistically similar P_b values across a range of size-fractioned biomass (picoplankton, nanoplankton and microplankton; although average P_b increased with decreasing cell size as expected) in both spring and summer in the Eastern Bering Sea despite the common observation that small cells have higher biomass-specific productivities due to reduced

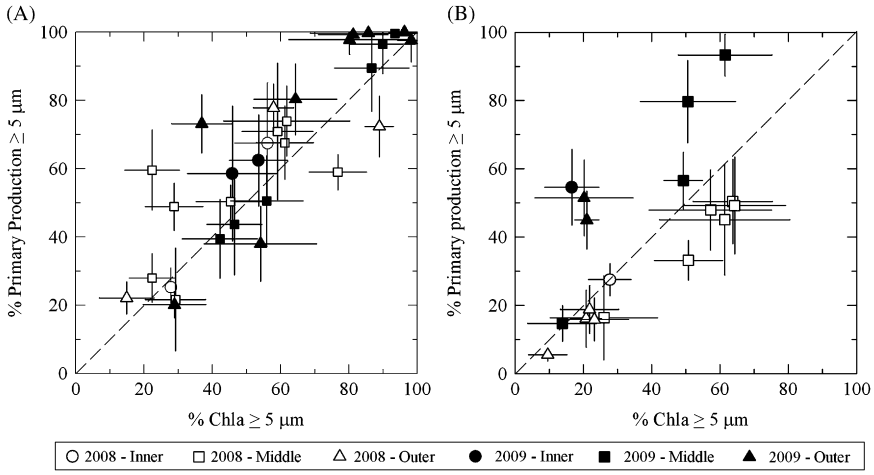

Fig. 10. Percent total primary production ≥5 µm vs. percent total Chl-a ≥5 µm separated by season, (A) spring and (B) summer. Each data point represents a separate process station and is the mean (±stdev.) of the seven sample depths.

influence of the package effect (Malone et al., 1993). Shiomoto et al. (1997) concluded that picoplankton P_b was decreased (as opposed to microplankton biomass-specific productivity being elevated), and was controlled by temperature in the Bering Sea, whereas microplankton productivity was not controlled by temperature. This suggests that microplankton are more adapted to low temperatures and might therefore be particularly susceptible to increases in temperature. The dataset presented here supports the findings of Shiomoto et al. (1997). At the macroscale, data presented here highlight the seasonal shift of the Bering Sea from a biomass-controlled production system (i.e., high and variable biomass, but low growth rates) to a growth-rate controlled production system, which has probable implications for a warmer Bering Sea and the flow of carbon and energy to, and ultimately the success of, higher trophic levels (Legendre and Michaud, 1998; Moran et al., 2012). For example, it has been hypothesized that *Calanus* spp., a dominant zooplankton grazer in this region, has highest recruitment and survival in cold years due to increased availability of large size, high quality phytoplankton prey (Baier and Napp, 2003; C. Ashjian and R. Campbell, pers. comm.). Furthermore, it has been suggested that warming temperatures will likely enhance water column stratification (Coyle et al., 2008) increasing the likelihood of nutrient-stress and a reduction in phytoplankton growth rates, reduced microzooplankton biomass and grazing rates and possible reductions in large zooplankton which graze heavily on microzooplankton throughout the year, but especially in the summer (Strom and Fredrickson, 2008).

4.2. Estimates of shelf wide annual productivity

Considering the economic importance of the fisheries resources within the Eastern Bering Sea, and suggestions of the impact of climate change on this ecosystem (e.g., Coyle et al., 2008; Schumacher et al., 2003; Strom and Fredrickson, 2008), it is paramount that we understand the environmental control of ecosystem productivity and its temporal and spatial variability. To understand the mechanisms controlling ecosystem productivity, information is needed not only on the partitioning of carbon and energy within the lower trophic levels (e.g., Moran et al., 2012), but also on the absolute amount of carbon and energy entering the system at the first trophic level, NPP. The former can be approached geochemically (e.g., net community production, NCP) based on net seasonal change in inorganic carbon, nutrients, and/or oxygen; Mathis et al., 2010). The latter can be approached biologically by directly measuring rates of NPP and autotrophic biomass as we have accomplished. Geochemical estimates of NCP are attractive as they inherently average over large time and space scales, however there are a number of important assumptions particularly with regard to along-shelf and across-shelf flow and freshwater inputs in dynamic coastal shelf systems (Mathis et al., 2010). Direct biological measurements of NPP (e.g., using isotopic incubations) and biomass are more labor and resource intensive (i.e., incubations are often a day in length as in this study), and do not integrate over the same time and space scales as the geochemical estimates. As a result, direct observational datasets of NPP still remain sparse.

More importantly, both geochemical and biological methods for measuring productivity have difficulties in quantifying the impact of small-scale variability on production (e.g., localized enhancement of productivity due to an eddy feature; Mizobata and Saitoh, 2004), which may be disproportionately important in estimating ecosystem productivity and/or channeling the flow of carbon and energy to higher trophic levels. The 2009 ice-edge bloom time-series is an example of the importance of localized enhancement of productivity. During that short bloom period alone, NPP was $\sim$55 g C m^{-2}. This value is one-third to one-half the average annual areal estimate of NPP provided by Rho and Whitledge (2007) for the region between the Pribilof Islands and the Aleutian chain (100–150 g C m^{-2} yr^{-1}), and would represent a significant underestimate of seasonal NPP if not measured and/or included in annual calculations derived from direct biological measurements. This 'burst' of productivity does not appear to be reflected in spatial maps of inorganic carbon based net community production (NCP) (see Fig. 6, Cross et al., 2012) where NCP in this region is much lower than in other regions of the Middle domain, both north and south, where measured NPP was lower than in the ice edge bloom. Furthermore, the $\sim$55 g C m^{-2} produced during this period would equate to a production of $\sim$0.8–1.1 g Chl-a m^{-2}, based upon the C:Chl-a values discussed below, and when added to the $\sim$0.3 g Chl-a m^{-2} that was present at the beginning of the time period of interest Chl-a was expected to be $\sim$1.1–1.4 g Chl-a m^{-2}. The fact that Chl-a accumulated to only $\sim$1 g Chl-a m^{-2} suggests that a large proportion of the production, 0.1–0.4, from this bloom was removed from the euphotic zone as the bloom was progressing. This is a key observation as generally high-biomass blooms are characterized by a temporal uncoupling of production and export (e.g., Buesseler, 1998). Moran et al. (2012) in 2008 observed export ratios (carbon export divided by carbon production) of $\sim$0.1 in the marginal ice zone bloom in 2008, although the ice-edge bloom in 2008 was not as well sampled as the bloom in 2009. Preliminary analysis of the 2009 field data suggests a higher export ratio was associated with the 2009 bloom (Moran, pers. comm.) which is more in line with the 0.1–0.4 export proportion implied

from Chl-a accumulation. Furthermore, a preliminary analysis of pigments captured in sediment traps suggests that early in the bloom the majority (>85%) of pigmented material was derived from direct settling of phytoplankton (phaeophoride+phaeophytin concentrations <15% of Chl-a concentrations at trap depths below the mixed layer; M. Baumann, M.W. Lomas, S.B. Moran, unpubl. data). At the end of the bloom period the phaeophorbide+phaeophytin concentrations had increased to ~30% of Chl-a perhaps suggesting a larger importance of grazers on organic material export at the end of the bloom (see also Moran et al., 2012).

Satellite-based approaches are commonly used to solve the temporal/spatial NPP sampling problem, allowing more detailed study of marine ecosystems (Yoder et al., 2010). These approaches hold many advantages, as well as disadvantages. In the Bering Sea, the extensive cloud cover can lead to substantial data gaps in satellite-based datasets, and groundtruthing and quantifying subsurface Chl-a maxima remain important problems in validating satellite products. Particularly as it has recently been shown that there is a consistent summer-time subsurface Chl-a maximum in the Northern Bering Sea (Stabeno et al., 2012-a). A VGPM-based upon underway ship data, such as presented here, has the advantage of not being influenced by cloud cover and easy access to samples for validation. Any 'remote' productivity model for the Bering Sea needs to at least consider subsurface Chl-a maxima and the impact this would have on estimating NPP from surface data, especially as subsurface Chl-a maxima are not always present or spatially uniform (i.e., northern vs. southern domains). However, the significant relationship between surface and euphotic zone integrated Chl-a (Fig. 8) suggests that for this study region and time period euphotic zone Chl-a could be predicted with reasonable confidence from surface Chl-a over much of the shelf.

Springer et al. (1996) were one of the first, and the most commonly cited, to synthesize estimates of annual Bering Sea productivity at the first trophic level (Table 3). NPP was estimated to be ~102 Tg (Tg=10^{12} g) C yr^{-1} partitioned as 23, 47, and 32 Tg C yr^{-1} for the Outer, Middle, and Inner domains, respectively. For the relatively warm years of 1999–2000, annual NPP in the Outer domain was estimated to be 48–67 Tg C yr^{-1} using satellite-derived input parameters and a VGPM identical in structure to that presented here (Mizobata and Saitoh, 2004). Unfortunately, Mizobata and Saitoh did not provide a comparison of model output (either estimates of Chl-a or NPP) with measured data so there is no independent validation to know if the higher values they observed in warm years represents a real elevation in productivity in the Outer Domain or problem in model validation. Comparing data from Rho et al. (2005) at the shelf break and mid-shelf (their Figs. 6 and 7) with data presented by Mizobata and Saitoh (2004; their Fig. 5) for the same years suggests that the satellite-derived outputs may be higher than ^{13}C-incubation values. For the period of 1997–1999 (mix of cool (1997, 1999) and warm (1998) years) Outer domain production was estimated to be 29 Tg C yr^{-1} based on data reported by Rho and Whitledge (2007), and twice that, 52 Tg C yr^{-1}, for the cold period from 1978–1981. Estimates provided by Rho and Whitledge (2007) were averaged over different areas of the shelf and are not focused on the 'Green Belt', which may explain the discrepancy between the two methods. Regardless, while models based either on remotely sensed or other nontraditional properties are clearly an attractive approach to obtain the spatial coverage needed to evaluate changes over areas as large as the Bering Sea shelf, ground truth measurements are crucial in their utility to evaluate temporal patterns in system parameters.

Similarly, two-fold differences between NPP in warm and cold years for other domains were reported by Rho and Whitledge (2007). For the entire shelf ecosystem, production was estimated from data in Rho and Whitledge (2007) to be 94 Tg C yr^{-1} during the mix of cool and warm years of 1997–1999 and 150 Tg C yr^{-1} for the cold years of 1978–1981. For the cold years of this present study, NPP was estimated to be between 106 Tg C yr^{-1} (geochemical estimate for 2008 only; Mathis et al., 2010) and 152 Tg C yr^{-1} (average of process station data, assuming 150 d productivity season split 50/50 between spring and summer cruise data as in Sambrotto et al., 2008 and summed across the six regions/domains). Applying the VGPM with the underway data (Fig. 11), shelf wide production was estimated to be 114 Tg C yr^{-1} (Table 4). This estimate is lower than the process station dataset, likely due to averaging of more data points not associated with the production hotspots near ice-edge blooms. In summary, estimated shelf-wide annual production, using similar methods, suggests there could be a factor of two higher productivity during cold years than warm years (Rho and Whitledge, 2007), however the difference between each method for a given region and block of years is also two-fold (cf. Rho and Whitledge, 2007; Mizobata and Saitoh, 2004). Based upon this analysis, NPP would have to change by greater than two-fold in response to climate change before it would be detectable against the high inherent variability in the Bering Sea.

A potential explanation for the estimated differences in shelf-wide NPP between cold and warm years (Table 4) could be related to a shift from biomass to growth rate control of production as waters warm. Warming temperatures may result in decreased nutrient input to the euphotic zone (due to temperature-dependent stratification in the southern region, cf. Ladd and Stabeno, 2012) and/or a shift to smaller cells. This shift to smaller cells may likely shunt a larger proportion of carbon and energy to

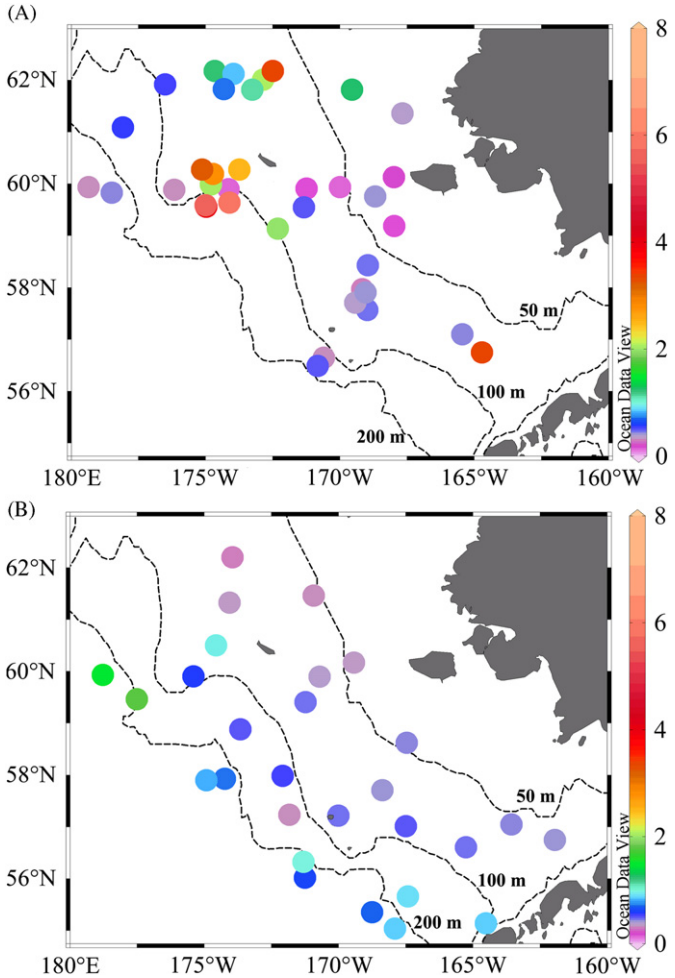

Fig. 11. VGPM calculated NPP (g C m^{-2} d^{-1}) using underway and meteorological data as inputs. (A) cruise HLY0902 and (B) cruise KN195. Each dot is centered on the mid day geographic position of a 24-h period corresponding to the VGPM estimates.

Table 4
Summary of annual primary production (Tg C yr^{-1}) estimates.

Study year	Outer Domain	Middle Domain	Inner Domain	Total shelf	Reference
	23	47	32	102	Springer et al. (1996)
1978–1981 (Cold)	52	54	44	150	Rho and Whitledge (2007)
1997–1999 (Cool/warm)	29	29	36	94	Rho and Whitledge (2007)
1998–2000 (Warm)	48–67	–	–	–	Mizobata and Saitoh (2004)
2008 (Cold)	20	50	36	106	Mathis et al. (2010)
2008–2009 (Cold)	59	49	44	152	This study, ^{14}C-incubations
2008–2009 (Cold)	43	47	24	114	This study, VGPM

microzooplankton which are rapid and efficient grazers of phytoplankton. Rose and Caron (2007) clearly show that the growth rates of herbivorous protists are more temperature sensitive than those of phototrophic protists. At cold ($<5\,^{\circ}C$) temperatures, growth rates of herbivorous protists are less than half those of phototrophic protists and at warmer temperatures growth rates converge on equal values or are even higher for herbivorous protists. Studies in several temperate ecosystems have shown that warmer temperatures during the course of a diatom-dominated spring bloom have led to overall lower NPP as a result of enhanced heterotrophic activity (Keller et al., 1999; Lomas et al., 2002). Not only may NPP decrease, but an increasingly large fraction of NPP derived carbon may be shunted to the dissolved organic carbon pool further reducing the carbon and energy available to higher trophic levels (Wohlers et al., 2009). It is also plausible that the dissolved organic carbon that accumulates does so because it is refractory (i.e., deplete of nitrogen and/or phosphorus) and therefore could represent a 'dead end' for the flow of carbon through the ecosystem (Thingstad et al., 1997). Changes in NPP linked to increasing temperature will undoubtedly be associated with changes in the flow of carbon through the lower trophic levels of the ecosystem and likely be associated with a reduction in carbon and energy available to higher trophic levels, even if NPP were to increase, due to the greater temperature sensitivity of heterotrophs.

Acknowledgments

We thank the officers and crew of the USCG Icebreaker *Healy* and R/V *Knorr* for their efforts and professionalism, the Chief Scientists for their tireless efforts to ensure successful cruises, and all the other BEST-BSIERP PI's who participated on the cruises and provided thought provoking conversations. We thank Scott Hiller of SIO, Steve Roberts of UCAR, and the Marine Technicians for the R/V *Knorr* for keeping CTD and underway systems running; Dave Kachel of PMEL, Nancy Kachel of UW/JISAO, Jessica Cross and Dan Naber of UAF for help in sampling; Eric Wisegarver of PMEL and Fred Menzia of UW/JISAO for running additional chlorophylls. This research was supported primarily by awards ARC-0732359 (MWL) and ARC-0732680 (SBM). This is BIOS Contribution number 2014 and BEST-BSIERP Contribution number 46. This is Contribution no. 3652 from the Pacific Marine Environmental Laboratory, NOAA and contribution EcoFOCI-0770 to NOAA's Fisheries—Oceanography Coordinated Investigations.

References

Aguilar-Islas, A., Rember, R., Mordy, C., Wu, J., 2008. Sea ice-derived dissolved iron and its potential influence on the spring algal bloom in the Bering Sea. Geophys. Res. Lett. 35, L24601. doi:10.1029/2008GL035736.
Baier, C., Napp, J., 2003. Cimate-induced variability in *Calanus marshallae* populations. J. Plankton Res. 25, 771–782.
Behrenfeld, M.J., Falkowski, P.G., 1997. Photosynthetic rates derived from satellite-based chlorophyll concentration. Limnol. Oceanogr. 42, 1–20.
Bradley, P.B., Lomas, M.W., Bronk, D.A., 2010. Phytoplankton uptake of inorganic and organic nitrogen in Chesapeake Bay measured using a flow cytometric approach: correction for bacterial uptake. Estuaries Coasts. doi:10.1007/s12237-009-9252-y.
Buesseler, K., 1998. The decoupling of production and particulate export in the surface ocean. Global Biogeochem. Cycles 12, 297–310.
Campbell, R., Sherr, E., Ashjian, C., Plourde, S., Sherr, B., Hill, V., Stockwell, D., 2009. Mesozooplankton prey preference and grazing impact in the western Arctic Ocean. Deep-Sea Res. II 56, 1275–1289.
Casey, J., Lomas, M., Aucan, J., 2011. Interannual dynamics of carbon partitioning within the Sargasso Sea picoplankton assemblage. In: Proceedings of ASLO Aquatic Sciences Meeting. San Juan, Puerto Rico.
Coachman, L.K., 1986. Circulation, water masses, and fluxes on the Southeastern Bering Sea shelf. Cont. Shelf Res. 5, 23–108.
Coachman, L.K., Charnell, R., 1979. On lateral water mass interaction—a case study, Bristol Bay, Alaska. J. Phys. Oceanogr. 9, 278–297.
Coyle, K.O., Pinchuk, A.I., Eisner, L.B., Napp, J.M., 2008. Zooplankton species composition, abundance and biomass on the Eastern Bering Sea shelf during summer: the potential role of water column stability and nutrients in structuring the zooplankton community. Deep-Sea Res. II 55, 1775–1791.
Cross, J., Mathis, J., Bates, N., 2012. Hydrographic controls on net community production and total organic carbon distributions in the Eastern Bering Sea. Deep-Sea Res. II 65–70, 98–109.
DuRand, M., Olson, R., 1996. Contributions of phytopankton light scattering and cell concentration changes to diel variations in beam attenuation in the equatorial Pacific from flow-cytometric measurements of pico-, ultra-, and nanoplankton. Deep-Sea Res. II 43, 891–906.
DuRand, M., Olson, R., Chisholm, S., 2001. Phytoplankton population dynamics at the Bermuda Atlantic time-series study station in the Sargasso Sea. Deep-Sea Res. II 48 (8–9), 1983–2003.
Fernandez, E., Maranon, E., Moran, X.A.G., Serret, P., 2003. Potential causes for the unequal contribution of picophytoplankton to total biomass and productivity in oligotrophic waters. Mar. Ecol.—Progr. Ser. 254, 101–109.
Geider, R.J., 1987. Light and temperature dependence of the carbon to chlorophyll a ratio in microalgae and cyanobacteria: implications for physiology and growth of phytoplankton. New Phytol. 106, 1–34.
Graham, H., Edwards, R., 1962. The world biomass of marine fishes. In: Heen, E. (Ed.), Primary Production in the Sea. Plenum Press, New Jersey, pp. 433–460.
Guo, L.D., Tanaka, T., Wang, D., Tanaka, N., Murata, A., 2004. Distributions, speciation and stable isotope composition of organic matter in the Southeastern Bering Sea. Mar. Chem. 91 (1–4), 211–226.
Hansell, D.A., Goering, J.J., Walsh, J.J., McRoy, C.P., Coachman, L.K., Whitledge, T.E., 1989. Summer phytoplankton production and transport along the shelf break in the Bering Sea. Cont. Shelf Res. 9 (12), 1085–1104.
Hillebrand, H., Durselen, C.-D., Kirschtel, D., Pollingher, U., Zohary, T., 1999. Biovolume calculation for pelagic and benthic microalgae. J. Phycol. 35, 403–424.
Hunt, G.J., Drinkwater, K., 2005. GLOBEC Symposium on Climate Variability and Sub-Arctic Marine Ecosystems. GLOBEC Newsletter 11. p. 14–17.
Hunt, G.J., Stabeno, P., Strom, S., Napp, J.M., 2008. Patterns of spatial and temporal variation in the marine ecosystem of the Southeastern Bering Sea, with special reference to the Pribilof domain. Deep-Sea Res. II 55, 1919–1944.
Hunt Jr., G.L., Bond, N., Stabeno, P., Ladd, C., Mordy, C., Whitledge, T., Feely, R., Mathis, J., Shull, D., Devol, A., Eisner, L., Sherr, E., Strom, S., Napp, J., Coyle, K.O., Mueter, F., Baker, T., Buck, G., Eggers, D.M., Stepanenko, M.A., Gritsay, E.V., Byrd, G.V., Fitzgerald, S., Allen, D., Angliss, R., Burkanov, V., Friday, N., Fritz, L., Gelatt, T., Lewis, W., Shelden, K., Sterling, J., Towell, R., Waite, J., 2010. Status and trends of the Bering Sea region, 2003–2008. In: McKinnell, S., Dagg, M. (Eds.), The Marine Ecosystems of the North Pacific Ocean; Status and Trends, 2003–2008. PICES, pp. 196–267.
Hunt Jr., G.L., Coyle, K.O., Eisner, L., Farley, E.V., Heintz, R., Mueter, F., Napp, J.M., Overland, J.E., Ressler, P.H., Salo, S., Stabeno, P.J., 2011. Climate impacts on Eastern Bering Sea food webs: a synthesis of new data and an assessment of the Oscillating Control Hypothesis. ICES J. Mar. Sci. 68, 1230–1243.
Hunt, G.L., Stabeno, P., Walters, G., Sinclair, E., Brodeur, R.D., Napp, J.M., Bond, N.A., 2002. Climate change and control of the Southeastern Bering Sea pelagic ecosystem. Deep-Sea Res. II 49 (26), 5821–5853.
IPCC, 2007. Climate Change 2007—Impacts, Adaptation and Vulnerability. Working Group II Contribution to the Fourth Assessment Report of the IPCC. Cambridge University Press, London.
Kachel, N.B., Hunt, G.L., Salo, S.A., Schumacher, J.D., Stabeno, P.J., Whitledge, T.E., 2002. Characteristics and variability of the inner front of the Southeastern Bering Sea. Deep-Sea Res. II 49 (26), 5889–5909.
Kameda, T., Ishizaka, J., 2005. Size-fractionated primary production estimated by a two-phytoplankton community model applicable to ocean color remote sensing. J. Oceanogr. 61, 663–672.

Keller, A.A., Oviatt, C.A., Walker, H.A., Hawk, J.D., 1999. Predicted impacts of elevated temperature on the magnitude of the winter-spring phytoplankton bloom in temperate coastal waters: a mesocosm study. Limnol. Oceanogr. 44, 344–356.
Kinder, T., Coachman, L.K., 1978. The front overlying the continental slope in the Eastern Bering Sea. J. Geophys. Res. 83, 4551–4559.
Knap, A., Michaels, A., Steinberg, D., Bahr, F., Bates, N., Bell, S., Countway, P., Close, A., Doyle, A., Howse, F., Gundersen, K., Johnson, R., Little, R., Orcutt, K., Parsons, R., Rathbun, C., Sanderson, M., Stone, S., 1997. BATS Methods Manual Version 4. U.S. JGOFS Planning Office, Woods Hole.
Koblentz-Mishke, O., Volkovinsky, V., Kabanova, I., 1970. Plankton primary production in the world ocean. Sci. Explor. S. Pac., 183–193.
Ladd, C., Stabeno, P.J., 2012. Stratification on the Eastern Bering Sea Shelf Revisited. Deep-Sea Res. II 65–70, 72–83.
Lee, S., Fuhrman, J., 1987. Relationship between biovolume and biomass of naturally derived marine bacterioplankton. Appl. Environ. Microbiol. 53, 1298–1303.
Legendre, L., Michaud, J., 1998. Flux of biogenic carbon in oceans: size dependent regulation by pelagic food webs. Mar. Ecol. Prog. Ser. 164, 1–11.
Lomas, M., Steinberg, D., Dickey, T., Carlson, C., Nelson, N., Condon, R., Bates, N., 2010. Increased ocean carbon export in the Sargasso Sea is countered by its enhanced mesopelagic attenuation. Biogeosciences 7, 57–70.
Lomas, M.W., Lipschultz, F., Nelson, D.M., Bates, N.R., 2009. Biogeochemical responses to late-winter storms in the Sargasso Sea. I. Pulses of primary and new production. Deep-Sea Res. I 56, 843–860.
Lomas, M.W., Glibert, P.M., Shiah, F.-K., Smith, E.M., 2002. Microbial processes and temperature in Chesapeake Bay: current relationships and potential impacts of regional warming. Global Change Biol. 8, 51–70.
Lorenzen, C., 1970. Surface chlorophyll as an index of the depth, chlorophyll content and primary productivity of the euphotic layer. Limnol. Oceanogr. 15, 479–480.
Malone, T., Pike, S., Conley, D., 1993. Transient variations in phytoplankton productivity at the JGOFS Bermuda time-series station. Deep-Sea Res. I 40 (5), 903–924.
Malone, T.C., 1980. Algal size. In: Morris, I. (Ed.), The Physiological Ecology of Phytoplankton. Blackwell Scientific, Oxford, pp. 433–463.
Maranon, E., Holligan, P., Barciela, R., Gonzalez, N., Mourino, B., Pazo, M., Varela, M., 2001. Patterns of phytoplankton size structure and productivity in contrasting open-ocean environments. Mar. Ecol. Prog. Ser. 216, 43–56.
Marra, J., 2002. Approaches to the measurement of plankton production. In: le, B., Williams, P.J., Thomas, D., Reynolds, C.S. (Eds.), Phytoplankton Productivity: Carbon Assimilation in Marine and Freshwater Ecosystems. Blackwell Science, Oxford, pp. 78–108.
Mathis, J., Cross, J., Bates, N., Moran, S., Lomas, M., Mordy, C., Stabeno, P.J., 2010. Seasonal distribution of dissolved inorganic carbon and net community production on the Bering Sea shelf. Biogeosciences 7, 1769–1787.
McRoy, C.P., Goering, J.J., 1976. Annual budget of primary production of the Bering Sea. Mar. Sci. Commun. 2, 255–267.
McRoy, C.P., Goering, J.J., Shiels, W., 1972. Studies of primary production in the eastern Bering Sea. In: Takenouti, A. (Ed.), Biological Oceanography of the Northern North Pacific Ocean. Idemitsu Shoten, pp. 199–216.
Meier, W., Stroeve, J., Fetterer, F., Knowles, K., 2005. Reductions in Arctic sea ice cover no longer limited to summer. EOS (Washington DC) 86, 326.
Menden-Deuer, S., Lessard, E.J., 2000. Carbon to volume relationships for dino-flagellates, diatoms, and other protist plankton. Limnol. Oceanogr. 45, 569–579.
Mizobata, K., Saitoh, S., 2004. Variability of Bering Sea eddies and primary productivity along the shelf edge during 1998–2000 using satellite multi-sensor remote sensing. J. Mar. Syst. 50 (1–2), 101–111.
Moran, S.B., Lomas, M.W., Kelly, R.P., Prokopenko, M., Granger, J., Gradinger, R., Iken, K., Mathis, J.T., 2012. Seasonal succession of net primary productivity, particulate organic carbon export, and autotrophic community composition in the Eastern Bering Sea. Deep-Sea Res. II 65–70, 84–97.
Mordy, C., Eisner, L., Proctor, P., Stabeno, P.J., Devol, A., Shull, D., Napp, J., Whitledge, T., 2010. Temporary uncoupling of the marine nitrogen cycle: accumulation of nitrite on the Bering Sea shelf. Mar. Chem. 121, 157–166.
Mordy, C., Stabeno, P., Righi, D., Menzia, F., 2008. Origins of the subsurface ammonium maximum in the Southeast Bering Sea. Deep-Sea Res. II 55, 1738–1744.
Motoda, S., Minoda, T., 1974. Plankton in the Bering Sea. In: Hood, D., Kelley, E. (Eds.), Oceanography of the Bering Sea. University of Alaska, Fairbanks, pp. 207–241.
Napp, J.M., Hunt, G.J., 2001. Anomalous conditions in the South-eastern Bering Sea 1997: linkages among climate, weather, ocean, and biology. Fish. Oceanogr. 10, 61–68.
Niebauer, H.J., Alexander, V., Henrichs, S., 1995. A time-series study of the spring bloom at the Bering Sea ice edge. I. Physical processes, chlorophyll and nutrient chemistry. Cont. Shelf Res. 15, 1859–1877.
Niebauer, H.J., Bond, N.A., Yakunin, L., Plotnikov, V., 1999. An update on the climatology and sea ice of the Bering Sea. In: Loughlin, T., Ohtani, K. (Eds.), Dynamics of the Bering Sea. University of Alaska Sea Grant, Fairbanks, pp. 29–60.
Overpeck, J.T., Sturm, M., Francis, J., Perovich, D., Serreze, M., Benner, R., Carmack, E., Chapin III, F., Gerlach, S., Hamilton, L., Hinzman, L., Holland, M., Huntington, H., Key, R., Lloyd, A., MacDonald, G., McFadden, J., Noone, D., Prowse, T., Schlosser, P., Vörösmarty, C., 2005. Arctic system on trajectory to new, seasonally ice-free state. EOS (Washington DC) 86 (309), 312–313.
Parsons, T., Maita, Y., Lalli, C., 1984. A Manual of Chemical and Biological Methods for Seawater Analysis. Pergamon Press, New York.
Rho, T., Whitledge, T.E., 2007. Characteristics of seasonal and spatial variations of primary production over the Southeastern Bering Sea shelf. Cont. Shelf Res. 27, 2556–2569.
Rho, T.K., Whitledge, T.E., Goering, J.J., 2005. Interannual variations of nutrients and primary production over the Southeastern Bering Sea shelf during the spring of 1997, 1998, and 1999. Oceanology 45 (3), 376–390.
Rose, J.B., Caron, D.A., 2007. Does low temperature constrain the growth rates of heterotrophic protists? Evidence and implications for algal blooms in cold waters. Limnol. Oceanogr.: Rev. 52, 886–895.
Saino, T., Miyata, K., Haqttori, A., 1979. Primary productivity in the Bering and Chukchi Seas and in the Northern North Pacific in summer 1978. Bull. Plankton Soc. Jpn. 26, 96–103.
Sambrotto, R., Niebauer, H.J., Goering, J.J., Iverson, R.L., 1986. Relationships among vertical mixing, nitrate uptake, and phytoplankton growth during the spring bloom in the southeast Bering Sea middle shelf. Cont. Shelf Res. 5, 161–198.
Sambrotto, R.N., Mordy, C.W., Zeeman, S.I., Stabeno, P.J., Macklin, S.A., 2008. Physical forcing and nutrient conditions associated with patterns of Chl a and phytoplankton productivity in the Southeastern Bering Sea during summer. Deep-Sea Res. II 55, 1745–1760.
Sarmiento, J.L., Slater, R., Barber, R.T., Bopp, L., Doney, S.C., Hirst, A., Kleypas, J.A., Matear, R., Mikolajewicz, U., Monfray, P., Soldatov, V., Spall, S., Stouffer, R., 2004. Response of ocean ecosystems to climate warming. Global Biogeochem. Cycles 18, GB3003. doi:10.1029/2003GB002134.
Schumacher, J.D., Bond, N.A., Brodeur, R.D., Livingston, P., Napp, J.M., Stabeno, P.J., 2003. Climate change in the Southeastern Bering Sea and some consequences for biota. In: Hempel, G., Sherman, K. (Eds.), Large marine Ecosystems of the World: Trends in Exploitation, Protection, and Research. Elsevier, Amsterdam, pp. 17–40.
Sherr, E., Sherr, B., Wheeler, P., Thompson, K., 2003. Temporal and spatial variation in stocks of autotrophic and heterotrophic microbes in the upper water column of the central Arctic Ocean. Deep-Sea Res. I 50, 557–571.
Shiomoto, A., Tadokoro, K., Monaka, K., Nanba, M., 1997. Productivity of pico-plankton compared with that of larger phytoplankton in the subarctic region. J. Plankton Res. 19 (7), 907–916.
Siegel, D., Dickey, T., 1987. On the parameterization of irradiance for open ocean photoprocesses. J. Geophys. Res.—Oceans 92, 14648–14662.
Sieracki, M., Verity, P., Stoecker, D., 1993. Plankton community response to sequential silicate and nitrate depletion during the 1989 North Atlantic spring bloom. Deep-Sea Res. II 40, 213–226.
Sorokin, Y.I., 1999. Data on primary production in the Bering Sea and adjacent Northern Pacific. J. Plankton Res. 21 (4), 615–636.
Springer, A.M., McRoy, C.P., Flint, M.V., 1996. The Bering Sea Green Belt: shelf-edge processes and ecosystem production. Fish. Oceanogr. 5, 205–233.
Sprules, W.G., Munawar, M., 1986. Plankton size spectra in relation to ecosystem productivity, size, and perturbation. Can. J. Fish. Aquat. Sci. 43, 1789–1794.
Stabeno, P., Farley, E., Kachel, N., Moore, S., Mordy, C., Napp, J., Overland, J., Pinchuk, A., Sigler, M., 2012a. A comparison of the physics of the northern and southern shelves of the eastern Bering Sea and some implications for the ecosystem. Deep-Sea Res. II 65–70, 14–30.
Stabeno, P., Moore, S., Napp, J., Sigler, M., Zerbini, A., 2012b. Comparison of warm and cold years on the Southeastern Bering Sea shelf and some implications for the ecosystem. Deep-Sea Res. II 65–70, 31–45.
Stabeno, P.J., Napp, J.M., Mordy, C.W., Whitledge, T., 2010. Factors influencing physical structure and lower trophic levels of the Eastern Bering Sea shelf in 2005: Sea ice, tides and winds. Prog. Oceanogr. 85, 180–196.
Stramski, D., Sciandra, A., Claustre, H., 2002. Effects of temperature, nitrogen and light limitation on the optical properties of the marine diatom *Thalassiosira pseudonana*. Limnol. Oceanogr. 47, 392–403.
Strom, S., Fredrickson, K., 2008. Intense stratification leads to phytoplankton nutrient limitation and reduced microzooplankton grazing in the Southeastern Bering Sea. Deep-Sea Res. II 55, 1761–1774.
Tamigneaux, E., Legendre, L., Klein, B., Minggelbier, M., 1999. Seasonal dynamics and potential fate of size-fractionated phytoplankton in a temperate nearshore environment (Western Gulf of St. Lawrence, Canada). Estuar. Coast. Shelf Sci. 48, 253–269.
Taguchi, S., 1972. Mathematical analysis of primary production in the Bering Sea in summer. In: Takenouti, A. (Ed.), Biological Oceanography of the Northern North Pacific Ocean. Idemitsu Shoten, pp. 253–262.
Thingstad, T., Hagstrom, A., Rassoulzadegan, F., 1997. Accumulation of degradable DOC in surface waters: is it caused by the malfunctioning microbial loop. Limnol. Oceanogr. 42, 398–404.
Tremblay, J., Legendre, L., 1994. A model for the size fractionated biomass and production of marine phytoplankton. Limnol. Oceanogr. 39, 2004–2014.
Tsiban, A., Korsak, M., 1987. Primary and microbial production in the Bering Sea. Biol. Sea (Vladisvostok) 6, 15–21.
Utermohl, H., 1958. Zur Vervollkommnung der quantitativen phytoplankton. Band 9, 1–38.
Vadrucci, M., Cabrini, M., Basset, A., 2007. Biovolume determination of phyto-plankton guilds in transitional water ecosystems of Mediterranean Ecoregion. Transitional Waters Bull. 2, 83–102.
Wohlers, J., Engel, A., Zollner, E., Breithaupt, P., Jurgens, K., Hoppe, H.-G., Sommer, U., Riebesell, U., 2009. Changes in biogenic carbon flow in response to sea surface warming. Proc. Acad. Nat. Sci. Philadelphia 106, 7067–7072.
Yoder, J., Doney, S., Siegel, D., Wilson, C., 2010. Study of marine ecosystems and biogeochemistry now and in the future: examples of the unique contributions from space. Oceanography 23, 104–117.